SANDIA REPORT
SAND2002-0183
Unlimited Release
Printed January 2002

Preliminary Investigation of the Thermal Decomposition of Ablefoam and EF-AR20 Foam (Ablefoam Replacement)

Tamara A. Ulibarri, Dora K. Derzon, Kenneth L. Erickson, Jaime Castaneda, Theodore T. Borek, Anita M. Renlund, Jill C. Miller, Daniel Clayton, and Thomas Fletcher

Prepared by
Sandia National Laboratories
Albuquerque, New Mexico 87185 and Livermore, California 94550

Sandia is a multiprogram laboratory operated by Sandia Corporation, a Lockheed Martin Company, for the United States Department of Energy under Contract DE-AC04-94AL85000.

Issued by Sandia National Laboratories, operated for the United States Department of Energy by Sandia Corporation.

Available to DOE and DOE contractors from
U.S. Department of Energy
Office of Scientific and Technical Information
P.O. Box 62
Oak Ridge, TN 37831

Telephone: (865)576-8401
Facsimile: (865)576-5728
E-Mail: reports@adonis.osti.gov
Online ordering: http://www.doe.gov/bridge

Available to the public from
U.S. Department of Commerce
National Technical Information Service
5285 Port Royal Rd
Springfield, VA 22161

Telephone: (800)553-6847
Facsimile: (703)605-6900
E-Mail: orders@ntis.fedworld.gov
Online order: http://www.ntis.gov/ordering.htm

SAND2002-0183
Unlimited Release
Printed January 2002

Preliminary Investigation of the Thermal Decomposition of Ablefoam and EF-AR20 Foam (Ablefoam Replacement)

Tamara A. Ulibarri
Physical Sciences Department

Dora K. Derzon
Organic Materials Aging and Reliability Department

Kenneth L. Erickson and Jaime N. Castaneda
Thermal, Fluid, and Aero Experimental Sciences Department

Theodore T. Borek
Materials Characterization Department

Anita M. Renlund and Jill C. Miller
Explosives Projects/Diagnostics Department

Sandia National Laboratories
P. O. Box 5800
Albuquerque, New Mexico 87185-0834

Daniel Clayton and Thomas H. Fletcher
Department of Chemical Engineering
Brigham Young University
Provo, Utah

ABSTRACT

Preliminary thermal decomposition experiments with Ablefoam and EF-AR20 foam (Ablefoam replacement) were done to determine the important chemical and associated physical phenomena that should be investigated to develop the foam decomposition chemistry sub-models that are required in numerical simulations of the fire-induced response of foam-filled engineered systems for nuclear safety applications. Although the two epoxy foams are physically and chemically similar, the thermal decomposition of each foam involves different chemical mechanisms, and the associated physical behavior of the foams, particularly “foaming” and “liquefaction,” have significant implications for modeling. A simplified decomposition chemistry sub-model is suggested that, subject to certain caveats, may be appropriate for “scoping-type” calculations.

CONTENTS

FIGURES

SUMMARY

Preliminary thermal decomposition experiments with Ablefoam and EF-AR20 foam (Ablefoam replacement) were done to determine the important chemical and associated physical phenomena that should be investigated to develop the foam decomposition chemistry sub-models that are required in numerical simulations of the fire-induced response of foam-filled engineered systems for nuclear and transportation safety applications. This work was done as part of the MAVEN Foam Project (Task 2: Foam Decomposition Chemistry Model Development), which provides input to the ASCI Weapon System / Subsystem Response Program.

This report first summarizes the experimental techniques and diagnostics used to examine foam decomposition. The results from the foam decomposition experiments then are discussed. Those results indicated that thermal decomposition of Ablefoam and EF-AR20 foam are controlled by different mechanisms. The experiments with Ablefoam indicated the following:

- Decomposition involves at least two, and probably three, major decomposition mechanisms. The major decomposition products are a variety of aromatic phenols. Some CO_2 also evolves during decomposition.

- At 300^o C, the vapor pressure of the decomposition products can exceed 1300 psia and can reasonably be expected to increase substantially with increasing temperature.

- During decomposition, about 20 to 30% of the original foam can be expected to form a thermally stable carbonized residue, which tends to occupy a major portion of the volume of the initial foam. The carbonized residue appears to maintain sufficient mechanical strength to retain its structure during a thermal event.

- Decomposition of the Ablefoam depends to some extent on confinement, or more precisely, depends on the rate of mass transfer of decomposition products away from the sample. However, this effect does not appear to be as severe as that observed with rigid polyurethane (RPU) foams.

- The physical behavior of the foam during decomposition can have severe modeling implications. In particular, softening or liquefaction of the decomposing foam and subsequent internal gas generation appear to cause “foaming” of the condensed-phase decomposition products that ultimately form the carbonized residue.

The experiments with EF-AR20 foam indicated the following:

- Decomposition involves at least two major decomposition mechanisms. The major decomposition products are a variety of aromatic phenols. Some H_2O and CO_2 also evolve under certain conditions.

- At 300^o C, the vapor pressure of the decomposition products can exceed 800 psia and can reasonably be expected to increase substantially with increasing temperature.

- During decomposition, about 5 to 10% of the original foam can be expected to form a thermally stable carbonized residue, which appears to be relatively fragile and may not have sufficient strength to maintain its structure during a thermal event.

- Decomposition of the EF-AR20 foam depends to some extent on confinement, or more precisely, depends on the rate of mass transfer of decomposition products away from the sample. However, this effect does not appear to be as severe as that observed with RPU foams.

- The physical behavior of the foam during decomposition can have severe modeling implications. In particular, liquefaction of the decomposing foam will occur at temperatures between about 370 to 380^{o} C and can result in the formation of substantial amounts of a freely flowing liquid phase that can have a substantial impact on heat transfer mechanisms.

Based on the above results, the following simplified decomposition mechanism, if used with caution, may be appropriate for "scoping-type" calculations.

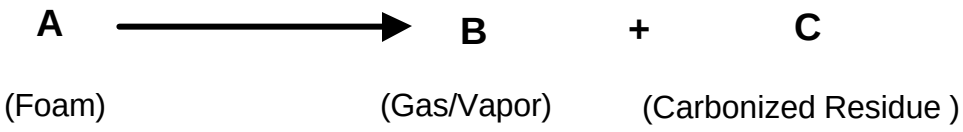

However, it should be carefully noted that:

- The above mechanism is a lumped representation of at least two mechanisms, and the decomposition chemistries of the Ablefoam and EF-AR20 foam have not been investigated in sufficient detail and are not yet well understood.

- The physical effects accompanying decomposition, particularly liquefaction of the EF-AR20 foam, can be substantial. For scenarios involving confined EF-AR20 foam and non-ablative heating conditions, substantial fluid flow during decomposition is likely, and the validity of calculations that neglect fluid flow should be viewed with caution.

This report has been provided to facilitate model development and guide further experimental work. Further work should be done to more completely define physical and chemical mechanisms.

INTRODUCTION

Preliminary thermal decomposition experiments with Ablefoam and EF-AR20 foam (Ablefoam replacement) were done to determine the important chemical and associated physical phenomena that should be investigated to develop the foam decomposition chemistry sub-models. Such models are required in numerical simulations of the fire-induced response of foam-filled engineered systems for nuclear and transportation safety applications. The experimental techniques and diagnostics used to examine thermal decomposition of Ablefoam and EF-AR20 foam were similar to those that have been used successfully to study the thermal decomposition of rigid polyurethane (RPU) foams[1] and to provide the data for developing an RPU foam decomposition chemistry sub-model.[2,3] The experimental techniques are briefly summarized below. The results obtained from the thermal decomposition experiments then are discussed, and a simplified decomposition chemistry sub-model is suggested that, subject to certain caveats, may be appropriate for demonstration-type calculations.

EXPERIMENT

Foam Samples

Experiments with Ablefoam were done with samples from MC2912, S/N 1889 (Arming, Fuzing, and Firing Assembly, or AF&F, for the W-76). Experiments with EF-AR20 were done with samples from lot P1711-73A produced at Sandia National Laboratories.[4] Some physical and chemical characteristics of the Ablefoam and EF-AR20 foam are similar; however, significant differences exist between the two foams. Results of analyses for total C, H, N, and O are given in Table 1.

Table 1. Total Carbon, Hydrogen, Nitrogen, and Oxygen Analyses.

Foam	C (wt. %)	H (wt.%)	N (wt.%)	O (wt.%)
Ablefoam	65.0	6.9	3.4	24.7
EF-AR20	71.3	8.5	3.0	17.2

Infrared microprobe spectra obtained using an ATR objective are shown in Figs. 1a and b for the initial Ablefoam and EF-AR20 foam samples, respectively. Optical and SEM micrographs showing the cell structure of the Ablefoam and EF-AR20 foam samples are shown in Figs. 2 and 3, respectively. Additional information concerning the Ablefoam and EF-AR20 foam is given in Refs. 5 and 6, respectively.

Experimental Techniques and Diagnostics

The experimental techniques and diagnostics used to study thermal decomposition of the Ablefoam and EF-AR20 foam are briefly described below. The techniques and diagnostics were selected to examine a broad range of temperatures, pressures, heating rates, and mass transfer rates that were imposed by various conditions of confinement.

Thermal Gravimetric Analysis (TGA) Experiments. Thermal gravimetric analysis (TGA) experiments with small (about 4- to 8-mg) samples were done in unconfined and partially confined sample configurations. The unconfined configuration involved samples in open platinum pans and was used to examine initial decomposition mechanisms under conditions that minimize effects of mass transfer and reversible and secondary reactions. The partially confined configuration involved sealed hermetic aluminum pans (TA Instruments) having lids with circular orifices as small as 0.06 mm. This configuration was used to examine the effects of any reversible or secondary reactions that would result from limiting mass transfer of the decomposition products.

The experimental arrangement for the TGA experiments is shown schematically in Fig. 4. Analysis of the gases that evolved from the samples, in either unconfined or partially confined configuration, most frequently was done real-time using Fourier Transform Infrared (FTIR) spectroscopy, as shown schematically in Fig. 4. The purge gas (typically 50 to 60 cc/min UHP N_2) from the TGA (TA Instruments Model 2950) furnace flowed through a heated stainless steel transfer line (maintained at 250 to 300^o C) to the TGA-FTIR Interface Unit in an Auxiliary Experiment Module (maintained at 300^o C) of a Nicolet Magna 750 FTIR Spectrometer.

An alternative technique, illustrated schematically by the dashed portion of Fig. 4, was used in selected experiments to obtain additional information for identifying several of the evolved gas species. In the alternative technique, periodic sampling of evolved gases was done using thermal desorption tubes connected directly to the exhaust from the TGA Furnace. The effluent end of the desorption tube was either vented or connected to the heated transfer line to the TGA-FTIR Interface Unit. Gas samples were collected on desorption tubes packed with Tenax TA, 60/80 mesh. In this case, the purge gas flow rate was approximately 30 cc/min. The desorption tubes were capped and placed in a Perkin-Elmer ATD400 Automated Thermal Desorption unit that was directly connected to a Finnigan GCQ gas chromatograph/ion trap mass spectrometer. The ATD400 is equipped with a Perkin-Elmer low-flow VOC trap for organic vapor concentration. The desorption tubes were heated to 350^o C to collect the sample gases on the trap. The trap was then heated to 350^o C to introduce the sample to the Finnigan GCQ gas chromatograph/ion trap mass spectrometer. The split ratio from the ATD400 was 40.6/1.3. The gas chromatography column used was a J&W DB-5ms 30 m x 0.25 mm capillary column, 1.0 µm film thickness. The GC heating profile was 40^o C for 7 minutes, then a 20 ^{o}C/min ramp to 295^o C, with a 5 minute hold at 295^o C. The mass spectrometer was used in the electron ionization mode (70 ev), one full scan per second was collected from mass 33 to 380. The filament delay time was 4.33 minutes.

Solid residues from the TGA pans were examined postmortem using a Nicolet NicPlan infrared microprobe (IRMP). The most useful spectra were obtained using an attenuated total reflectance (ATR) objective with a diamond crystal (Spectra Tech).

The TGA experiments were done using a variety of heating conditions, which included: (1) Constant heating rate of 20 ^{o}C/min, from ambient temperature to 775^{o} C or higher), (2) "one-step isothermal" consisting of a constant heating rate of 20 ^{o}C/min to a temperature of 400^{o} C, followed by a constant temperature period of about one hour or more, and (3) "two-step isothermal" consisting of a constant heating rate of 20 ^{o}C/min to a temperature of 300^{o} C, followed by a constant temperature period of two hours, then a constant heating rate of 20 ^{o}C/min to a temperature of 380^{o} C, followed by a second constant temperature period of two hours.

High-Pressure Thermal Gravimetric Analysis (HPTGA) Experiments. High-pressure foam pyrolysis experiments were done to determine the effects of pressure without the effects of confinement. The high-pressure TGA experiments were done with a DMT (Deutsche Montan Technologie) high pressure thermogravimetric analyzer (HPTGA) shown schematically in Fig. 5. The DMT HPTGA is electrically-heated and allows the control of temperature, pressure, gas concentrations, and flow rates. The temperature is monitored with thermocouples, while the pressure is controlled by a pressure control valve. The gas concentrations and flow rates are regulated with mass flow controllers. The HPTGA is controlled by a computer running TGAsoft® software, from DMT, to record the temperature, pressure, and sample weight as a function of time. The gas temperature near the sample is measured with the sample temperature thermocouple, and the sample temperature is assumed to be the same. Helium was used as the inert gas environment, due to its high thermal conductivity and low density, which should minimize the thermal delay and buoyancy effects, and hence increase the accuracy of the data. The buoyancy effects were of particular concern and necessitated the use of "blank" experiments to obtain mass versus time data to correct the sample mass versus time results for buoyancy effects.

Buoyancy was found to affect the blank experiments as a function of both temperature and pressure, especially during heating and cooling ramps. The blank results were subtracted from sample results to obtain data corrected for buoyancy effects. As shown in Fig. 6a, with the exception of the 1 bar data, the blanks appear to vary linearly with pressure. They have similar shapes and appear to be a function of the apparatus geometry. The blank runs were repeated between three to six times for each pressure. The blank experiments were very reproducible, as indicated in Fig. 6b. An average of the replicated blank experiments was used to correct the data from each sample experiment.

The samples of EF-AR20 foam were cut in thin slices from a block, resulting in sample sizes of 3.0 to 6.5 mg. The samples were held in a solid, circular basket constructed from a small cylinder of Incoloy metal. The basket weighs 1.5 g, with a diameter of 0.5 inches and a height of 0.25 inches. A handle was attached in order to

suspend the basket from the chain from the balance. The solid basket was necessary in order to handle the liquids formed during the pyrolysis of the EF-AR20 foam.

High-Pressure Cell Experiments. High-pressure cell, constant-load, piston-displacement experiments involving larger samples (about 50-100 mg) were used to examine decomposition under highly confined conditions, in which mass transfer is highly limited and the effects of any reversible or secondary reactions would be most significant. The experimental arrangement for examining the response of polyurethane foam to heating under confinement is shown in Fig. 7. Small foam samples (typically 0.5" diameter by 0.25" height) were heated inside a cylindrical steel cell between opposing pistons sealed with Viton o-rings. The top piston was allowed to move by a distance of up to 0.4" against a fixed applied load, with a constant force supplied by a pneumatic cylinder with loading force up to 100 lb. The bottom piston was threaded into a load cell to monitor the total load (resulting from both the load applied from the pneumatic cylinder and the load due to friction as the piston moved). The top piston usually contained a thermocouple to measure the surface temperature of the foam. The cell was heated with a band heater and cell temperatures were measured with thermocouples at four locations in the steel cell. The experiment was conducted with the assembly inside a vacuum chamber and with the valve to the pump nearly closed; thus any significant leak from the cell could be detected without interference from slow outgassing from the heated assembly itself. After heating, samples were extracted to allow postmortem examination for both chemical decomposition and morphology changes. Displacement of the movable piston, measured by a LVDT, and the force, measured by the load cell, were recorded and indicated both mechanical processes, e.g., compaction and chemical processes such as decomposition and gas evolution.

Tube Furnace Experiments. Tube furnace experiments were done with relatively large samples (about 5 g) to obtain data for reaction products and molecular weight distributions under intermediate conditions of confinement. The size of the foam samples used was large enough to limit mass transfer to the surrounding atmosphere. The apparatus for and the diagnostics used with the tube furnace experiments are shown schematically in Fig. 8. Cold traps were used to collect organic products for subsequent analysis. Due to the larger sample size, gel permeation chromatography (GPC) could be used to examine the molecular weight distributions of the condensates. In some experiments, periodic sampling and analysis of evolved gases were done using desorption tubes followed by GC-MS. The procedures for desorption tube sampling and GC-MS analysis were similar to those used in the TGA experiments discussed above. Condensates and furnace residues were examined postmortem using infrared microprobe (IRMP). Analyses of furnace residues were also obtained for C, H, N, and O.

Foam samples were pyrolyzed in quartz tubes at a heating rate of 5°C/min to 400, 500, or 600°C. Ultrapure nitrogen gas flowed through the system at a rate of 100ml/min. The outlet gases were cooled in dry ice/acetone traps at –78° C. Two traps were used in the initial experiment. Negligible residue was collected in the second trap. Therefore, in subsequent experiments, only one trap was used to facilitate changing flasks to collect condensate samples at different times during the experiment. The gas leaving the quartz

tube flowed through desorption tubes to provide samples for subsequent GC-MS analysis. Samples were taken with desorption tubes placed before or after the trap (Fig. 8).

Pyrolysis was carried out by Thermolyne model 211100 tube furnace. The ends of the furnace were packed with glass wool. Foam chunks with total weight of about 5 g were placed in the quartz tube, one layer thick, and positioned to be in the center 1/3 of the tube furnace. Glassware used for pyrolysis included two configurations. Both had Pyrex hose nipple-to-24/40 adapters as gas inlets. Pyrolysis tubes were either 28-mm ID by 55-cm long quartz with male 24/40 fittings, which incorporated an elbow, or were 38-mm ID by 44-cm long straight quartz with female 24/40 fittings and a separate 16.5mm ID quartz elbow. Female fittings were used in order to permit placing larger samples into the tube. Pyrex 500-ml three-neck round bottom flasks were used in the first and second cooling traps. The traps were connected through a custom-made 16-mm ID Pyrex U-tube. The flask in the final cooling bath was connected to a hose nipple outlet. Desorption tubes were added to some of the experiments by adding a glass three-way valve with Teflon stopcocks onto the outlet. This allowed for adjusting the flow rate through the desorption tubes to about 20-30ml/min.

Gas flow was regulated by an MKS 1179A mass flow controller and model 246 power supply readout. A check valve was installed between the mass flow controller and the quartz tube in order to prevent back-flow into the flow controller. Latex tubing was used to connect the check-valve to the glassware. Gas flow was measured at the outlet of the system prior to pyrolysis using a calibrated Omega FMA-5707 gas flow meter. To insure sealing of the galss joints, the joints that were heated during the experiment were secured with copper wires. The remaining joints were secured by Keck clips.

RESULTS

TGA

As mentioned above, TGA-FTIR experiments were done with both unconfined and partially confined samples of Ablefoam and EF-AR20 foam. Unless otherwise noted, the experiments were done with samples in powder form, which was obtained by grinding small pieces of each foam with a mortar and pestle. The powder particles had characteristic dimensions of 0.5 mm or less. The experiments with unconfined samples are discussed first, because they provide information on initial decomposition mechanisms under conditions that minimize effects of mass transfer and reversible and secondary reactions. The experiments with partially confined samples are then discussed to assess effects of mass transfer and reversible and secondary reactions. Essentially, similar experiments were done with both Ablefoam and EF-AR20 foam.

Ablefoam: Unconfined Samples. Constant heating rate experiments with unconfined samples were done to examine decomposition rates as a function of temperature. The samples were heated at 20 ^{o}C/min to about 775^{o} C or higher. The furnace purge rate was

about 50 to 60 cc/min. Results in terms of percent of the initial sample mass remaining versus temperature are shown in Fig. 9 for two physically different samples of Ablefoam. The corresponding temperature histories are shown in Fig. 10b. One sample consisted of five fragments having characteristic dimensions greater than 1 mm. The other consisted of a powder, obtained by crushing fragments with a mortar and pestle as mentioned above. Both samples produced very similar results, which indicate that for the samples used, particle size effects were small. Both samples produced residues containing about 20% of the original sample mass, and the residues were thermally stable to temperatures of about 975^{o} C. Furthermore, the physical behavior of the sample consisting of five fragments is worth noting. The particles decreased in volume, but maintained much of their original shape, and the relative decrease in volume was much less than 80%, which would correspond to the loss in mass of the particles. Similar and more measurable behavior was observed in the tube furnace experiments, which are discussed later.

More insight into foam decomposition can be obtained by examining the rate-of-mass-loss curve given by the derivative $\frac{d(m/m_0)}{dt}$ versus time or temperature. Figure 10a shows the rate-of-mass-loss (derivative) curves corresponding to the two samples represented in Fig. 9. The derivative curve is essentially a "double-peaked" curve, which indicates that at least two decomposition steps may occur. One shows a maximum decomposition rate at about 320^{o} C. The other shows a maximum rate at about 395^{o} C. Unfortunately, the FTIR spectra collected as a function of time during the TGA experiments with Ablefoam were generally not useful, due to low signal intensity, although the spectra did indicate that CO_2 was produced during decomposition. The low signal intensity may have been due to decomposition products condensing in the heated transfer line (maintained at 300^{o} C), and may indicate the evolution of relatively high molecular-weight decomposition products having low vapor pressures.

To investigate the decomposition process further, an isothermal decomposition experiment was done, in which gas samples were collected periodically using desorption tubes and were subsequently analyzed by GC-MS. Figures 11a and 11b show, respectively, the mass-loss curve and corresponding temperature history from a 6.9-mg sample of Ablefoam powder that was heated at 20^{o} C/min to about 400^{o} C and then maintained at 400^{o} C for 60 minutes. The value of m/m_0 decreases rapidly during the constant heating rate period and during about the first fifteen minutes of the isothermal period, after which time, the value of m/m_0 changes very slowly, and after 60 minutes at 400^{o} C, the value of m/m_0 is about 0.35, which is well above the final value of 0.20 in Fig. 9. Two gas samples were collected during the constant-heating-rate period, and another sample was collected during about the first fifteen minutes of the isothermal period, as indicated in Fig. 11a. Several products, primarily aromatic phenols and cresols were identified. However, further experiments are needed to obtain larger samples and to address high-molecular-weight products, which may be difficult to desorb from the packing in the desorption tubes.

The relatively long period between about 35 and 75 minutes, during which the value of m/m_0 in Fig. 11a changes very slowly and does not decrease below about 0.35, may

indicate that an additional decomposition mechanism is involved at temperatures above 400° C. The maximum values in the derivative curves in Fig. 10a occur between about 380 and 400° C and are about 15 %/min. Therefore, the value of m/m_0 in Fig. 11a could reasonably be expected to decrease to values near 0.2 by the end of the isothermal period. To investigate the possibility of an additional decomposition mechanism occurring at temperatures above 400° C, a two-step isothermal experiment using a 4.9-mg sample was done as follows: (1) The sample was heated at a constant rate of 20° C/min to 300° C; (2) this was followed by an isothermal period of 240 minutes at 300° C; (3) the sample was then heated again at a constant rate of 20° C/min to 380° C, and (4) this was followed by an isothermal period of 240 minutes at 380° C. The residue that remained in the sample pan at the end of the two-step experiment was allowed to cool to room temperature and was subsequently used in a constant heating rate experiment, in which the residue was heated at 20° C/min to about 775° C. The mass loss curve and temperature history for the two-step isothermal experiment are shown in Figs. 12a and 12b, respectively. The mass loss curve and temperature history for the subsequent constant-heating rate experiment is shown in Fig. 13 and the corresponding rate-of-mass-loss (derivative) curve and temperature history are shown in Fig. 14a and 14b, respectively.

In Fig. 12a, the value of m/m_0 decreases rapidly during the first constant-heating-rate period. This should be primarily due to the decomposition mechanism corresponding to the first "peak" in the derivative curves in Fig. 10. During the subsequent isothermal period, the value of m/m_0 continues to decrease more slowly, but does not appear to "flatten out." Decomposition during this period is probably governed by the mechanisms corresponding to both the first and second "peaks" in the derivative curves in Fig. 10. The value of m/m_0 again decreases rapidly during the second constant-heating-rate period. This should be primarily due to the decomposition mechanism corresponding to the second "peak" in the derivative curves in Fig. 10. During the second isothermal period, the value of m/m_0 continues to decrease rapidly for about 20 to 30 minutes, and this also should be primarily due to the decomposition mechanism corresponding to the second "peak" in the derivative curves in Fig. 6. However, after about the first 30 minutes of the second isothermal period, the value of m/m_0 begins decreasing much more slowly and almost "flattens out" at a value of about 0.45.

The mass-loss and derivative curves in Figs. 13 and 14a, respectively, show that negligible decomposition occurred in the residue from the two-step isothermal experiment at temperatures below 400° C. Above 400° C, the value of $\frac{d(m/m_0)}{dt}$ increases and reaches a maximum at about 500° C. However, about 73 percent of the residue, or about 34 percent of the original sample, still remains at a temperature of about 775° C. The amount of thermally stable residue remaining is similar to the amount remaining after the isothermal experiment at 400° C. This result may indicate that a relatively slow secondary reaction occurs, which produces a more thermally stable reaction product that ultimately forms carbonized residue. However, this reaction, if it occurs, probably would be of second order importance in all but very slow heating scenarios.

Ablefoam: Partially Confined Samples. The mass-loss and derivative curves from a constant-heating-rate (20^o C/min to 575^o C) experiment with a 3.8-mg sample of Ablefoam powder that was partially confined by a 0.06 mm orifice are shown in Figs. 15 and 16a, respectively. For comparison, the analogous curves for the unconfined powder sample shown in Figs. 9 and 10a are also shown in Figs. 15 and 16a, respectively. The corresponding temperature histories are shown in Fig. 16b. The mass loss curve in Fig. 15 indicates that decomposition of the Ablefoam depends to some extent on confinement, or more precisely, depends on the rate of mass transfer of decomposition products away from the sample. Since aluminum melts at 660^o C, the partially-confined experiments using hermetic aluminum pans and lids were terminated at lower temperatures than the unconfined experiments, which were done with open platinum pans. However, based on the shape of the curves in Fig. 15, the partially confined sample would probably have produced more carbonized residue than the unconfined experiment. This also is consistent with a relatively slower secondary reaction, as mentioned above, that produces a more thermally stable secondary product, which ultimately forms carbonized residue. The derivative curve in Fig. 16a more clearly shows that confinement altered the rate of decomposition. The decomposition step corresponding to the first "peak" occurs relatively more rapidly, and the decomposition step corresponding to the second "peak" occurs relatively more slowly. Furthermore, a sharp "spike" in the derivative curve, such as the one occurring at about 400^o C, generally indicates that the orifice in the aluminum lid plugged due to foaming or liquefaction of the sample. The plug subsequently released as a result of rapidly increasing gas pressure. Postmortem examination of the sample pans revealed a black continuous foam-like residue that appeared to fill the internal volume of the pan and lid. The cell structure of the residue was visible to the naked eye. The sample powder appears to have liquefied or severely softened and coalesced during decomposition at temperatures of about 400^o C. Internal gas/vapor generation then resulted in foaming of the material. This behavior also is consistent with the cell structure changes observed in the samples of Ablefoam used in the tube furnace experiments discussed later.

EF-AR20 Foam: Unconfined Samples. A constant heating rate experiment with an unconfined sample of EF-AR20 foam was done to examine decomposition rates as a function of temperature. The sample was heated at 20^o C/min to about 775^o C. The furnace purge rate was about 50 to 60 cc/min of UHP N_2. Results in terms of percent of the initial sample mass remaining versus temperature are shown in Fig. 17. For comparison, the curve for the analogous experiment with an unconfined sample of powdered Ablefoam (Fig. 9) is also shown in Fig. 17. The corresponding rate-of-mass-loss curves and temperature histories are shown in Fig. 18a and 18b, respectively.

The mass loss curves in Fig. 17 indicate significant differences in decomposition behavior between the EF-AR20 foam and the Ablefoam.The amount of residue left by the EF-AR20 foam was much less than that left by the Ablefoam, and physically, the residue left by the EF-AR20 foam was considerably different from that left by the Ablefoam. The residue from the EF-AR20 foam consisted of several small black particles adhering to the

bottom of the platinum pan. A portion of that material appeared to have solidified from a liquid. The volume of the residue was much smaller than that of the original sample and appeared to have decreased in approximately direct proportion to the mass lost from the sample.

The differences in decomposition behavior between the EF-AR20 foam and the Ablefoam can be further illustrated by examining the derivative curves shown in Fig. 18a. The derivative curve for the EF-AR20 sample also is essentially a "double-peaked" curve, which indicates that at least two decomposition steps may occur. However, in the case of the EF-AR20 foam, the "peaks" are well separated. The first smaller peak has a maximum at about 180^{o} C, while the other larger peak has a maximum at about 395^{o} C.

The FTIR spectra collected as a function of time during the TGA experiment with the EF-AR20 sample were much more useful than those collected with Ablefoam samples, although some problems with retention of decomposition products in the heated-transfer line appeared to persist. Selected spectra are shown in Fig. 19 and further indicate that at least two decomposition mechanisms exist. The spectra in Fig. 19 were assumed to represent a superposition of the spectra for several products. To identify possible major decomposition products, library searches were done using the Nicolet FTIR library and search program. The spectrum at about 10 minutes (Fig. 19a) is representative of the spectra obtained during the time interval corresponding to the first peak in Fig. 18a. A search using the Nicolet FTIR library indicated phenolic products. The best fit was obtained with nonylphenol (88.9% fit to the library spectrum). The spectrum at about 15 minutes (Fig. 19b) is representative of the time period between the two peaks in Fig. 18a and is significantly different from the spectrum at 10 minutes. A library search yielded a reasonable fit (85.6%) to ethylene glycol diacrylate. The spectra at about 20 minutes and greater in Figs. 19c-f are representative of the time period corresponding to the second peak. Those spectra essentially have the same features and are somewhat similar to the spectrum at 10 minutes. The spectrum at 20 minutes appears to indicate the presence of water above the level that might occur in the spectrum due to small fluctuations in background. A library search of the spectrum in Fig 17d also indicated phenolic products. The best fit was obtained with bisphenol-A (93.5% fit to the library spectrum), and a reasonably good fit was also obtained with nonylphenol (89.9%).

To investigate the decomposition process further, an isothermal decomposition experiment was done, in which gas samples again were collected periodically using desorption tubes and were subsequently analyzed by GC-MS. Figure 20a shows the mass loss curve for a 4.9-mg sample of EF-AR20 powder that was heated at 20^{o} C/min to about 400^{o} C and then maintained at 400^{o} C for 60 minutes. The corresponding temperature history is shown in Fig. 20b. In Fig. 20a, the value of m/m_0 decreases rapidly during the constant heating rate period and during about the first fifteen minutes of the isothermal period, after which time, the value of m/m_0 changes relatively slowly. After 60 minutes at 400^{o} C, the value of m/m_0 is about 0.09, which is well below the final value of 0.35 in Fig. 11 for the corresponding Ablefoam results. Furthermore, the value of m/m_0 in Fig. 20a is still decreasing gradually after 60 minutes at 400^{o} C. Two gas samples were collected during the constant-heating-rate period, and another sample was collected

during the first fifteen minutes of the isothermal period, as indicated in Fig. 20a. The first gas sample was collected as the foam sample was heated from ambient temperature to 250^{o} C. The major decomposition product was tentatively identified as nonylphenol. The second gas sample was collected as the foam was heated from 250 to 395^{o} C. The major products appeared to be low-molecular weight aromatic phenols, such as phenol, p-isopropyl phenol and 2-(2-propenyl) phenol. The third sample was collected for about 15 minutes after the temperature of the foam sample reached 395^{o} C. Again, the major products appeared to be low-molecular weight aromatic phenols, such as o-cresol and ethyl phenol. However, further experiments are needed to obtain larger samples and to address high-molecular-weight products which may be difficult to desorb from the packing in the desorption tubes.

EF-AR20 Foam: Partially Confined Samples. The mass-loss and derivative curves from a constant-heating-rate (20^{o} C/min to 575^{o} C) experiment with a, 4.3-mg sample of EF-AR20 foam powder that was partially-confined by a 0.06 mm orifice are shown in Figs. 21 and 22a, respectively. For comparison, the curves for the unconfined EF-AR20 sample shown in Figs. 17 and 18a are also shown in Figs. 21 and 22a, respectively. The corresponding temperature histories are shown in Fig. 22b. The mass loss curve in Fig. 21 indicates that confinement, or more precisely the rate of mass transfer of decomposition products away from the sample, has some effect on the decomposition of EF-AR20 foam. In particular, the early decomposition step, starting at about 180^{o} C, that was observed with the unconfined sample is suppressed under confinement, and the entire mass loss curve is shifted toward higher temperatures by about 25 ^{o}C. However, the difference in the amount of carbonized residue that formed with the confined and unconfined samples is small and may be within the range of sample-to-sample variation.

The derivative curve in Fig. 22a further shows that confinement alters the rate of decomposition. The decomposition step corresponding to the first “peak” is either absent or occurs with the decomposition step corresponding to the second “peak.” Since the second peak has significantly broadened, the two mechanisms may occur concurrently. Furthermore, the sharp “spike” that occurs in the derivative curve when the temperature is between about 370 to 380^{o} C, again probably indicates that the orifice in the aluminum lid had plugged due to foaming or liquefaction of the sample. The plug subsequently released as a result of rapidly increasing gas pressure. Postmortem examination of the sample pans revealed a black lacquer-like residue coating the internal surface of the pan and lid. The sample powder appears to have liquefied at temperatures of about 370^{o} C or less. Internal gas/vapor generation then resulted in fluid flow. This behavior is consistent with the total liquefaction observed in the samples of EF-AR20 used in the tube furnace experiments discussed later. Finally, selected FTIR spectra collected as a function of time during the partially-confined experiment are shown in Fig. 23. The spectra all essentially have the same features and indicate that the types and ratios of decomposition products changed little during decomposition. A library search again indicated aromatic phenolic products. The best fit was obtained with bisphenol-A (93.5% fit to the library spectrum), and a reasonably good fit was also obtained with nonylphenol (89.9% fit to the library spectrum).

High-Pressure Thermal Gravimetric Analysis (HPTGA)

EF-AR20 Foam: Unconfined Samples. A limited number of HPTGA experiments were done with EF-AR20 foam. Constant heating rate experiments with unconfined samples were done to examine decomposition rates as a function of temperature and pressure. The samples were heated at 20^{o} C/min to about 600^{o} C. Results in terms of percent of the initial sample mass remaining versus temperature are shown in Fig. 24 for several pressures from 1 to 50 bar. The mass loss curves shown are the average of replicate experiments. In general, as the pressure increases, the mass loss curves are shifted toward higher temperatures. The shift is comparable to that observed in comparing the mass loss curves for unconfined powdered samples and those partially-confined by a 0.06-mm orifice. However, in the case of the pressure results, even at 50 bar, the first decomposition step (that occurs at a temperature of about 180^{o} C) is still fairly prominent and may indicate a fundamental difference between the thermodynamic effects of pressure and the mass transfer and concentration effects of confinement.

Isothermal experiments also were done at 1 bar pressure in the HPTGA. The samples were heated at rates of 20 ^{o}C/min to temperatures of 300, 350, or 400^{o} C and then held at constant temperature for 2 hours. The resulting mass loss curves and temperature histories are shown in Figs. 25a and 25b, respectively.

To examine the physical behavior of the foam, samples were heated at rates of 20 ^{o}C/min to temperatures of 300, 350, 400 or 450^{o} C and then cooled to 200^{o} C within 10 s. The residue remaining in the basket was photographed immediately after the experiment. The photographs were obtained using a low-intensity microscope with a magnification of about 30x. Photographs from samples after heating to 300 and 350^{o} C are shown in Figs. 26a and 26b, respectively. The foam cell structure in both figures appears to be reasonably well intact. However, some cell enlargement or incipient bubble formation appears to have occurred at 350^{o} C. Photographs from two different samples after heating to 400^{o} C are shown in Figs. 27a and 27b, respectively. In Fig. 27a, distortion of the foam cell structure is apparent and bubble formation or liquefaction appears to have been imminent. In Fig. 27b, liquefaction obviously had occurred. This result is consistent with both results from the preceding partially-confined TGA experiment in which liquefaction occurred at temperatures between about 370 and 380^{o} C and the results from the tube furnace experiments discussed below. A photograph from a sample heated to 450^{o} C is shown in Fig. 28. The sample obviously had liquefied.

High-Pressure Cell

As mentioned above, high-pressure cell experiments were done with samples of both Ablefoam and EF-AR20 foam. Residues from the experiments were examined using the IRMP with the ATR objective.

Ablefoam. The results from an experiment with Ablefoam are shown in Fig. 29, which includes data for applied load, piston displacement, temperature, and gas/vapor pressure as a function of time. Postmortem examination of the residue in the cell indicated a black, brittle, foam-like material, the physical appearance of which was much different than the original sample. Figure 30a shows the IRMP spectrum from the residue, and Fig. 30b shows the spectrum from the initial Ablefoam. While the two spectra share similar features, obvious differences exist, indicating that significant decomposition occurred at 300^{o} C. Furthermore, the pressure data in Fig. 29 show a maximum pressure of over 1300 psia. At higher temperatures, much higher pressures could be expected due to the intrinsic effect of temperature and a probable trend toward the formation of lower average molecular weight gas/vapor decomposition products.

EF-AR20 Foam. The results from an experiment with EF-AR20 foam are shown in Fig. 31, which includes data for applied load, piston displacement, temperature, and gas/vapor pressure as a function of time. The step-like nature of the load and pressure curves are believed to be a result of the piston sticking due to liquefaction of the sample. Postmortem examination of the residue in the cell revealed a soft brown-to-black material that appeared to have formed from a liquid state during cooling. The material remained soft and wax-like after cooling to room temperature. Figure 32a shows the IRMP spectrum from the residue, and Fig. 32b the spectrum from the initial EF-AR20 foam. While the two spectra share some similar features, major differences exist, which indicate that significant decomposition occurred at 300^{o} C. Furthermore, the maximum gas/vapor pressure (not shown in Fig. 31) observed in the experiment was about 800 psia. Again at higher temperatures, much higher pressures could be expected due to the intrinsic effect of temperature and a probable trend toward the formation of lower average molecular weight gas/vapor decomposition products.

Tube Furnace

Ablefoam: Partitioning to Solids, Liquids, and Gases. Multiple tube furnace Ablefoam degradation experiments were completed. The Ablefoam pieces were taken from MC2912, S/N 3447 and S/N 1869 (Arming, Fuzing, and Firing Assembly, or AF&F, for the W-76). Even though the runs were completed on pieces from different origin, the results were fairly consistent, implying that the Ablefoam manufacture was relatively well controlled.

The first information examined was the partitioning of the degradation products into solids, liquids, and gases. It was desirable to determine these results from much larger samples than those used in the TGA or high-pressure cell experiments. While there was some variance in the resulting partitioning between residual solids, condensable liquids and the gaseous by-products, most likely due to slight differences in the thermal ramp characteristics, the different runs led to fairly reproducible results. Some representative data are presented in Table 2. In general there was a large amount of liquid generated (>50 wt %), a moderate amount of residual solid material (~30 wt %) and a small amount of gaseous material (~10 wt %).

Table 2. Partitioning of Products in Ablefoam Decomposition.

Experiment #	Wt % Residual (solid)	Wt % Condensables (liquid)	Wt % Volatiles (gas)
081398 (DKDII-27)	31.4%	57.5%	11.1%
020399 (DKDII-71)	28.8%	64.5%	6.7%
040699 (DKDIII-6)	29.7%	51.8%	18.4%

In all cases the samples were heated at a temperature ramp of 5 °C/min. In the experiment # 081398 a final set-point of 400 °C was used, and in the other experiments a set-point of 500 °C was used. The two later experiments were examined in more detail by collecting different fractions of the condensable materials. See Tables 3 and 4 for each respective experiment.

Table 3. Fractions of Condensable Material Collected in #020399.

Flask or Container	Temperature Range (°C)	Mass of Condensate Collected (g)	Wt % of Original Sample
Flask 1	Ambient – 250 plus 30 min hold	0.767	14.1
Flask 2	250 – 350	0.819	15.1
Flask 3	350 – 400	0.904	16.7
Flask 4	400-500	0.503	9.3
Flask 5	500 hold	0.089	1.6

Table 4. Fractions of Condensable Material Collected in #040699.

Flask or Container	Temperature Range (°C)	Mass of Condensate Collected (g)	% of Original Sample
Flask 1	Ambient - 320	0.879	16.7
Flask 2	320 - 350	0.458	8.7
Flask 3	350 – 500 plus 4 hour hold	1.387	26.4

The partitioning of the Ablefoam sample between solid, liquid and gas during thermal degradation is consistent with the larger samples providing partial self confinement that hinders mass transport of the degradation products away from the sample.

Ablefoam Gas: Chromatography/Mass Spectrometry (GC-MS) Analysis. In order to identify the volatile organic species evolved from the thermal degradation of Ablefoam, six desorption tube samples were collected during a thermal degradation experiment as shown in Figure 33a. The TGA data was used to determine the sampling times as shown in Figure 33b. The actual desorption tube sample points are given in Table 5.

Table 5. Desorption Tube Sample Points for Ablefoam.

Tube ID	Initial Temperature (°C)	Final Temperature (°C)	Sample Duration (minutes)
XL	13	13	13
XM	325	350	5
XX	380	405	5
XZ	425	450	5
XY	550	575	5
XW	600	600	5

The resulting analysis of the different tube contents produced very similar product identifications. For the most part, the volatiles are comprised of small aromatic and

phenolic compounds. Compounds detected by GC-MS were toluene, benzene, xylene, phenol, ortho- and para-cresol, 2,6-dimethylphenol, 2,4-dimethylphenol, trimethylphenol (tentative assignment), and ethylmethylphenol (tentative assignment). Figure 34a depicts the total ion chromatogram(TIC) for tube XZ and Figures 34b-g show some of the corresponding chemical identifications of individual scans.

Ablefoam: Pyrolyzed Foam Analysis. Since Ablefoam retains a slight odor after pyrolysis, it was of interest to determine the volatile components, if detectable. Both GC-MS and elemental analysis were used to examine the pyrolyzed Ablefoam. Two different methods were used to complete GC-MS headspace analysis on a pyrolyzed piece of Ablefoam. The first method used a piece of pyrolyzed foam in an unpacked glass desorption tube. The material was then placed into the thermal desorption unit and was heated to evolve gases directly for analysis. The resulting total ion chromatogram (TIC) is shown in Figure 35. There were two very weak signals that are identified by scan number. The mass spectra were too weak to permit identification, nor did the species/scan numbers correspond to any known compounds previously analyzed.

The second method to determine the headspace gases involved placing a small amount of the pyrolyzed foam in a test tube and exposing the test tube atmosphere to a TENAX packed desorption tube, as shown in Figure 36. The headspace was passively sampled for 7 days, then the tube was analyzed. No peaks were observed.

Elemenatal analysis was completed on both the original Ablefoam material and the pyrolyzed Ablefoam. Table 6 compares the two sets of elemental analysis data.

Table 6. Elemental Analysis Data for Original and Pyrolyzed Ablefoam.

Element Analyzed For	Original Ablefoam, %	Pyrolyzed Ablefoam, %
C	65.0	85.4
H	6.9	1.9
N	3.4	6.4
O	24.7	6.3

The extremely high carbon content and low hydrogen content of the pyrolyzed Ablefoam is indicative of complete degradation to a carbonized, nonvolatile product. This information taken with the GC-MS analysis indicates that the tube furnace pyrolysis reactions are being taken to completion and that the odor is from trace amounts of a highly odiferous organic compound.

Ablefoam: Cell Structure Change. In order to determine cell structure change of the Ablefoam with increasing temperature, 4 pieces (MC 2912, S/N 1160) of comparable size were placed in a quartz tube, as shown in Fig. 37, with an UHP N_2 flow rate of 100 cc/min. The pieces were heated at a rate of 5°C/min. with a Thermolyne 79300 clamshell furnace. A cold trap was attached to the system to condense the condensable off-gases. Pieces were removed at selected temperatures up to 600°C. The clamshell furnace was used to allow viewing of the pieces while removing them. The foam pieces were heated to 350°C and one piece was quickly removed with a long spatula while the temperature of the furnace was held constant. As soon as the piece was removed, the furnace was closed and allowed to recover to the set temperature. This required about 2 to 5 minutes for each removal process. Heating was continued, and one piece was removed at 450°C; another was removed at 550°C, and the fourth was removed after being heated for four hours at 600°C.

The foam piece removed at 350°C appeared to be in a semi-liquefied state with the original cell structure intact. When touched by the spatula the piece deformed slightly and stuck to it. The sample re-solidified after cooling. The second piece, which was removed at 450°C, was hard and had to be forced off the tube wall. The inside had very large voids while the outsides appeared to remain intact. At 550°C the sample was hard and "puffed out." All three of the pieces removed from the furnace tube had a very strong phenolic odor. Further heating to 600°C with a four-hour hold did not change appearance, but the phenolic odor was gone. Optical microscopy images were taken before heating and after the 600°C, 4-hour bake. The foam appears to shrink approximately 33% in length and width as shown in Fig. 38. Cell structure changes dramatically upon heating. Large voids form in the center of the piece and reduce in size toward the surfaces, as shown in Fig. 39.

EF-AR20 Foam: Partitioning to Solids, Liquids, and Gases. Two tube furnace experiments were done with the EF-AR20 foam. Both experiments involved samples having a rectangular cross section of one cm^2 and a length of 10 cm (sample masses of about 5.2 to 5.5 gm). The furnace was set at a heating rate of 5^o C/min for both samples, and the furnace tube was purged with UHP N_2 at a flow rate of 100 ml/min.

As with the Ablefoam experiments, the EF-AR20 experiments were very reproducible. Data from one of the experiments are discussed below. The first information examined is the partitioning between residual solids, condensable liquids and the gaseous by-products. As shown in Table 7, EF-AR20 gave very different results than Ablefoam. There is appreciably less residual material from a pyrolysis experiment with EF-AR20 and significantly more condensable liquid material.

Table 7. Partitioning of Products in EF-AR20 versus Ablefoam.

Sample	Wt% Residual (solid)	Wt% Condensables (liquid)	Wt% Volatiles (gas)
EF-AR20 (021799)	2.2%	91.4%	6.4%
Ablefoam 020399	28.8%	64.5%	6.7%

As with the Ablefoam experiments, the EF-AR20 pyrolysis reaction was examined in more detail by collecting fractions during the pyrolysis experiment. The furnace was heated at 5 ^{o} C/minute to 500^{o} C and then maintained at that temperature for 3.5 hr. Four flasks were used to collect products over specified temperature intervals as indicated in Table 8.

Table 8. Fractions of Condensable Material Collected in Experiment 021799 with EF-AR20 Foam.

Flask or Container	Temperature Range (^{o} C)	Mass of Condensate Collected (g)	% of Original Sample
Flask 1	Ambient – 220	0.088	1.7
Flask 2	220 – 320	0.565	10.9
Flask 3	320 – 400	2.265	43.7
Flask 4	400 – 500 plus 20 minute hold	0.072	1.4

Since some condensation occurred in the transfer line to the trap, both the quartz tube in the furnace and the transfer line were tilted slightly downward to prevent liquid from accumulating at the joint between the quartz tube and the transfer line. At temperatures between 320 and about 377^{o} C, an obvious amount of liquid flowed from the quartz tube into the transfer line and Flask 3. At the conclusion of the experiment, it was found, that the entire sample in the furnace had liquefied, and that most of it had collected in Flask 3 or condensed in the transfer line. Specifically, 1.748 g , or 33.73%, of the original sample were removed from the transfer line. As indicated in Table 7 only 0.112 g (2.2%) of the sample remained in the quartz tube, and 6.4% of the original sample appeared to form either light gases or vapors that did not condense in the trap. Liquefaction of the sample seriously perturbed the experiment above 320^{o} C, and subsequent analysis of the contents of the four flasks provided only limited insight into the decomposition chemistry.

Additionally, GPC analysis of the contents of the flasks was completed. Flask 2 indicated four peaks corresponding to molecular weights (within a factor of about 2, relative to a polystyrene standard) of 359, 486, 766, and 1636, which indicates the presence of monomer and dimer units from the parent epoxy material. Analysis of two different fractions of Flask 3 was completed, as well as flask 4. The bulk of Flask 3 showed the presence of similar monomer and dimer materials. However, in the less

liquid portion of flask 3, some higher molecular weight fractions were detected, namely, 2330, 3121 and 6700. These molecular weights indicate the presence of fragments containing 4, 6 and 12 coupled monomer units. Flask 4 contained only monomer and dimer materials.

The GC-MS analyses of the collected condensate materials showed a large number of products. However, many of the peaks in the total ion chromatogram (TIC) overlapped or were irregular in shape. Therefore, the mass spectra obtained probably represented mixtures of constituents and were not useful for product identification. Furthermore, some evidence indicated that the chromatographic column may have contained residual contamination from preceding analyses.

The results from FTIR analysis of the contents in the flasks are shown in Fig. 40. Spectra from two samples taken from Flask 1 are shown in Fig. 40a and 40b; spectra from two samples taken from Flask 2 are shown in Fig. 40c and 40d; spectra from three samples taken from Flask 3 are shown in Fig. 40e to 40g, and spectra from three samples taken from Flask 4 are shown in Fig. 40h to 40j. Some differences occur between the spectra corresponding to Flask 1 and 2, but most of the spectral features are very similar and indicate similar decomposition products. The spectra corresponding to Flask 3 show further changes, some of which should be due to the liquefaction products flowing to the flask. Still further changes are evident in the spectra from Flask 4. Library searches for each of the spectra in fig. did not produce good agreement with any library spectra. However, the search results did indicate a variety of possible phenol-type products, particularly nonylphenol

EF-AR20 Foam: GC-MS Analysis During Pyrolysis. In order to identify the volatile organic species evolved during the thermal degradation of EF-AR20, eight desorption tube samples were collected during a thermal degradation experiment. The TGA data were used to determine the sampling times as shown in Figure 41. The actual desorption tube sample points are given in Table 9.

Table 9. Desorption Tube Sample Points for EF-AR20.

Tube ID	Initial Temperature (^{o} C)	Final Temperature (^{o} C)	Sample Duration (minutes)
XS	13	13	20
XT	200	250	10
XU	250	300	10
XV	300	350	10
XW	375	395	4
XX	395	400	1
XY	475	525	10
XZ	600	600	5

The GC-MS data from the desorption tubes proved far more informative than the condensate analysis. The first tube (XS) had a very weak signal, as expected for a room temperature sample. There was only one peak in the total ion scan (TIC) at 349 and it appeared to be toluene. Tube XT showed peaks indicative of siloxanes and nonyl phenol. Tube XU also contained nonyl phenol, as well as benzene, toluene, phenol, isopropyl phenol, 2(2-propenyl) phenol, butylated hydroxytoluene, 4-pyridinamine (tentative assignment), as well as some unidentified scans. Tube XV showed a decrease in higher boiling species (i.e., the higher molecular materials such as nonyl phenol were not present), and in general showed a decrease in overall signal intensity. Lower molecular weight siloxanes appeared to be present. Benzene, toluene, phenol, aniline and some other nitrogen ring species, such as pyridinamine and pyrimidine-type chemicals were definitely present. Tubes XW and XX had definitely diminished signals and only toluene and xylene were observed. Tube XY showed toluene, xylene and phenol. By increasing the temperature to 600^{o} C for tube XZ, the toluene, xylene and phenol signals seen in the last few tubes were still seen, but also derivatized phenols, such as cresol and isopropyl phenol were also observed.

In general, the GC-MS data indicates the production of a range of aromatic compounds being generated during the thermolysis reaction. These compounds include simple aromatics, such as benzene and toluene, to phenolic and ring N-containing species.

Pyrolyzed EF-AR20 Analysis. The residual pyrolyzed material was submitted for elemental analysis to compare to Ablefoam. As shown in Table 10, while the foams show very different solid, liquid, gas partitioning and very different physical behavior, the residual material is very similar in chemical composition. In essence, both materials leave a highly carbonaceous char material.

Table 10. Elemental Analysis of Char Material for EF-AR20 versus Ablefoam.

Analyzed Element	Original EF-AR20, %	Charred EF-AR20, %	Charred Ablefoam, %
C	71.3	88.2	85.4
H	8.5	1.9	1.9
N	3.0	4.6	6.4
O	17.2	5.3	6.3

DISCUSSION, CONCLUSIONS, AND RECOMMENDATIONS

These results indicated that thermal decomposition of Ablefoam and EF-AR20 foam involve different mechanisms. The experiments with Ablefoam indicated the following:

- Decomposition involves at least two, and probably three, major decomposition mechanisms. The major decomposition products are a variety of aromatic phenols. Some CO_2 also evolves during decomposition.

- At 300^{o} C, the vapor pressure of the decomposition products can exceed 1300 psia and can reasonably be expected to increase substantially with increasing temperature.

- During decomposition, about 20 to 30% of the original foam can be expected to form a thermally stable carbonized residue, which tends to occupy a major portion of the volume of the initial foam. The carbonized residue appears to maintain sufficient mechanical strength to retain its structure during a thermal event.

- Decomposition of the Ablefoam depends to some extent on confinement, or more precisely, depends on the rate of mass transfer of decomposition products away from the sample. However, this effect does not appear to be as severe as that observed with RPU foams.

- The physical behavior of the foam during decomposition can have severe modeling implications. In particular, softening or liquefaction of the decomposing foam and subsequent internal gas generation appear to cause "foaming" of the condensed-phase decomposition products that ultimately form the carbonized residue.

The experiments with EF-AR20 foam indicated the following:

- Decomposition involves at least two major decomposition mechanisms. The major decomposition products are a variety of aromatics, phenols, and some nitrogen aromatic compounds. Some H_2O and CO_2 also evolve under certain conditions.

- At 300^{o} C, the vapor pressure of the decomposition products can exceed 800 psia and can reasonably be expected to increase substantially with increasing temperature.

- During decomposition, about 5 to 10% of the original foam can be expected to form a thermally stable carbonized residue, which appears to be relatively fragile and may not have sufficient strength to maintain its structure during a thermal event.

- Decomposition of the EF-AR20 foam depends to some extent on confinement, or more precisely, depends on the rate of mass transfer of decomposition products away from the sample. However, this effect does not appear to be as severe as that observed with RPU foams.

- The physical behavior of the foam during decomposition can have severe modeling implications. In particular, liquefaction of the decomposing foam will occur at temperatures between about 370 to 380^{o} C and can result in the formation of substantial amounts of a freely flowing liquid phase.

Based on the above results, the following simplified decomposition mechanism, if used with caution, may be appropriate for "demonstration-type" calculations.

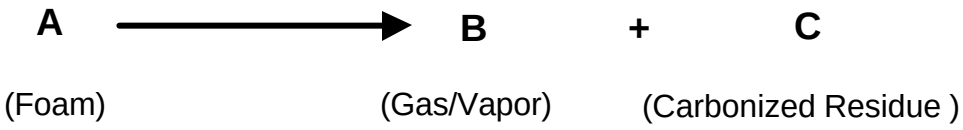

However, it should be carefully noted that:

- The above mechanism is a lumped representation of at least two mechanisms, and the decomposition chemistries of the Ablefoam and EF-AR20 foam have not been investigated in sufficient detail and are not yet well understood.

- The physical effects accompanying decomposition, particularly liquefaction of the EF-AR20 foam, can be substantial. For scenarios involving confined EF-AR20 foam and non-ablative heating conditions, substantial fluid flow during decomposition is likely, and the validity of calculations which neglect fluid flow should be viewed with caution.

ACKNOWLEDGEMENTS

The authors gratefully acknowledge the assistance provided by E. M. Russick (Org. 1811).

REFERENCES

1. K. L. Erickson, et al., in preparation.

2. T. Y. Chu, M. L. Hobbs, K. L. Erickson, et al., "Fire-Induced Response in Foam Encapsulants," *1999 SAMPE '99 - 44th International SAMPE Symposium & Exhibition*, Long Beach, CA, May 24-27, 1999.

3. M. L. Hobbs, K. L. Erickson, and T.Y. Chu, "Modeling Decomposition of Unconfined Rigid Polyurethane Foam," *Polymer Degradation and Stability*, **69**, 47 (2000).

4. Sample provided by E. M. Russick, Sandia National Laboratories.

5. W. E. Richardson, G. K. Baker, and C. R. Stanley, *The Synthesis of a Low-Density Rigid Epoxy Foam*, BDX-613-407, Bendix, Kansas City Division, March 1971.

6. Edward M. Russick and Peter B. Rand**,** *Development and Characterization of a New Epoxy Foam Encapsulant as an Ablefoam Replacement*, SAND98-2538, Sandia National Laboratories, December 1998.

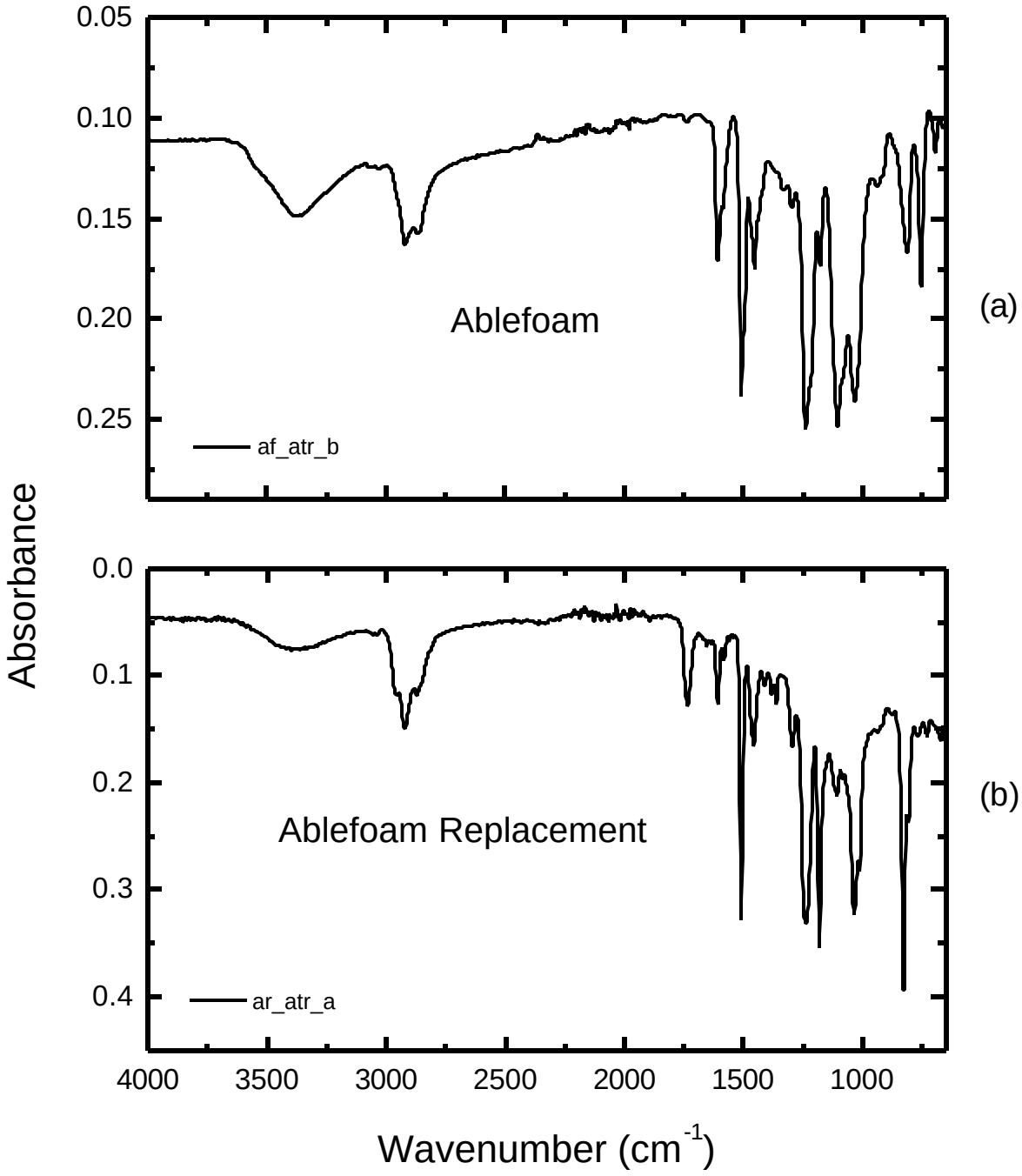

Fig. 1. Infrared microprobe spectra obtained using an ATR objective: (a) the initial Ablefoam sample and (b) the initial EF-AR20 foam sample.

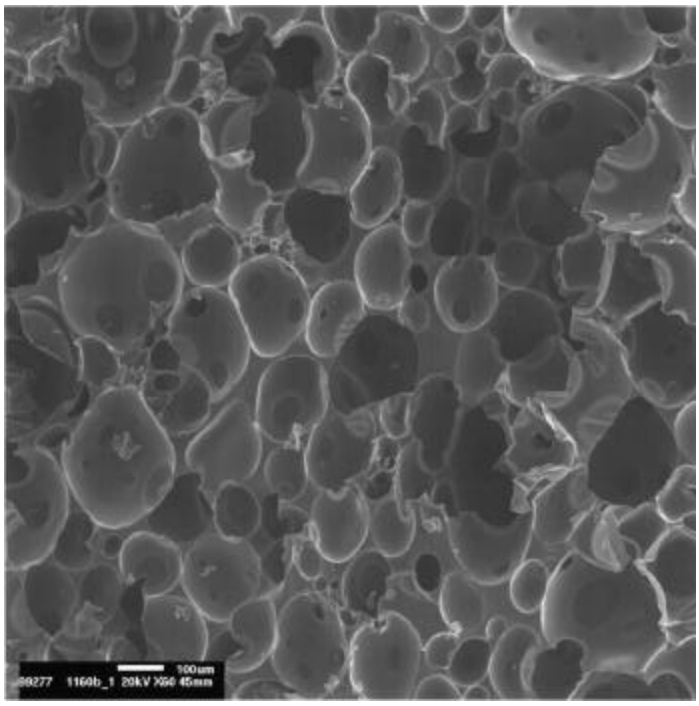

Fig. 2. Optical micrograph showing the cell structure of the Ablefoam.

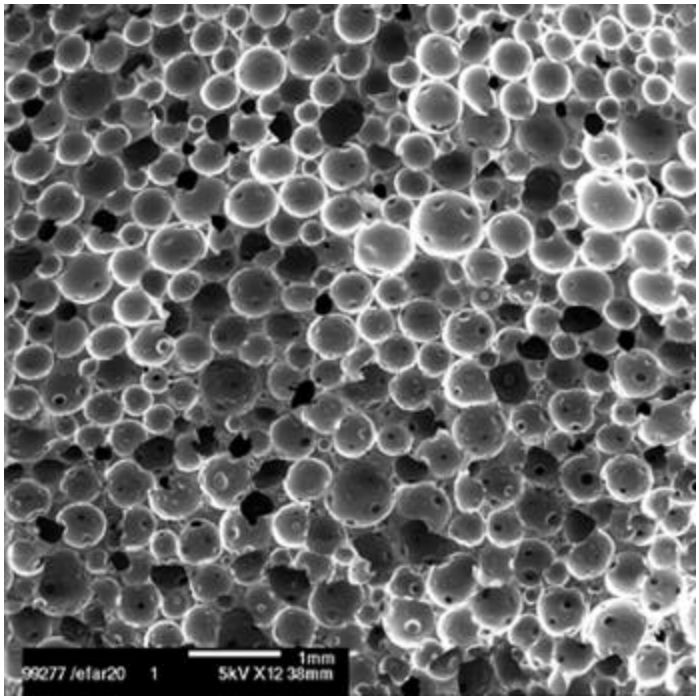

Fig. 3. SEM micrograph showing the cell structure of the EF-AR20 foam.

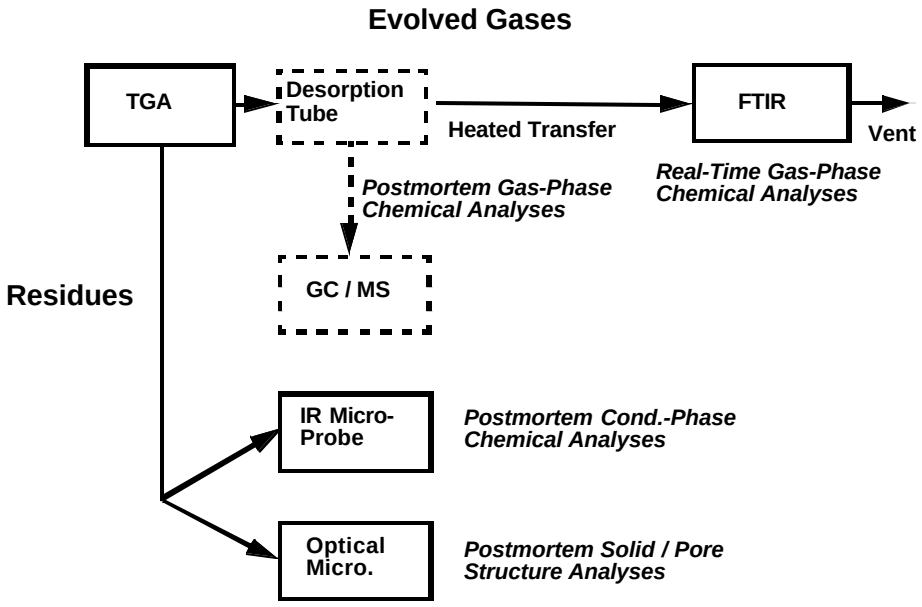

Fig. 4. Schematic diagram of the TGA-FTIR experiments.

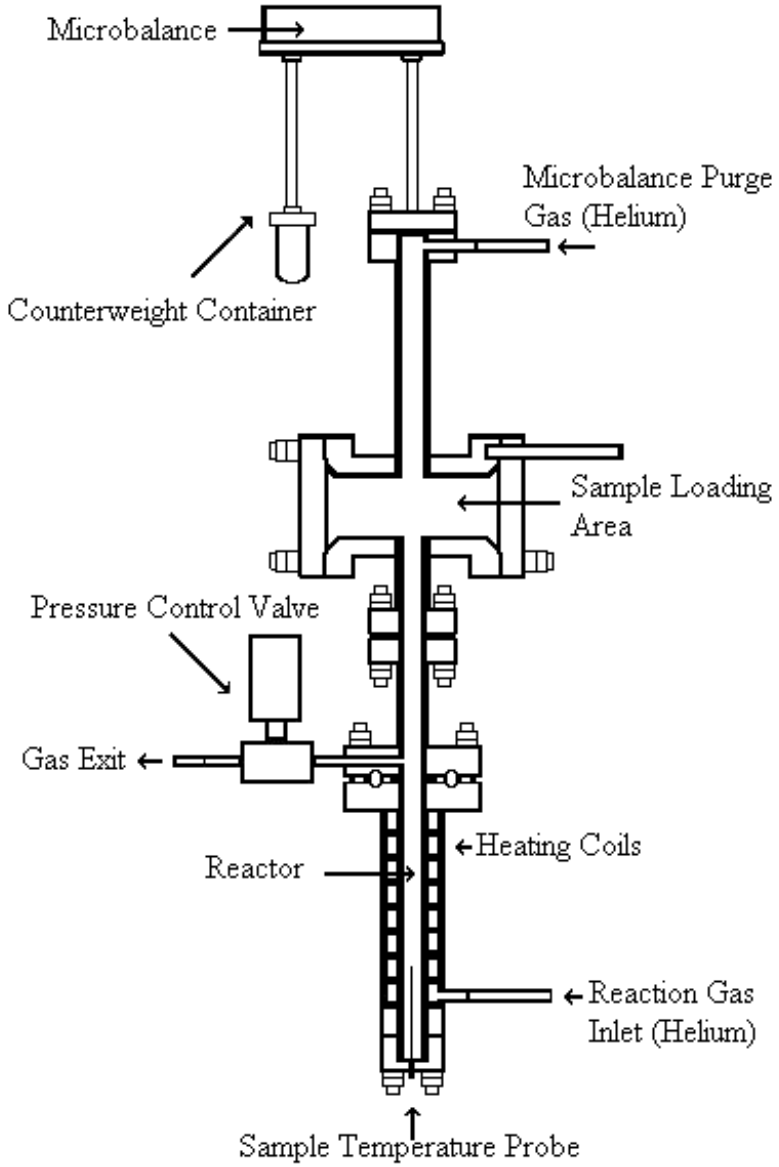

Fig.5. Schematic diagram of the DMT high pressure thermogravimetric analyzer.

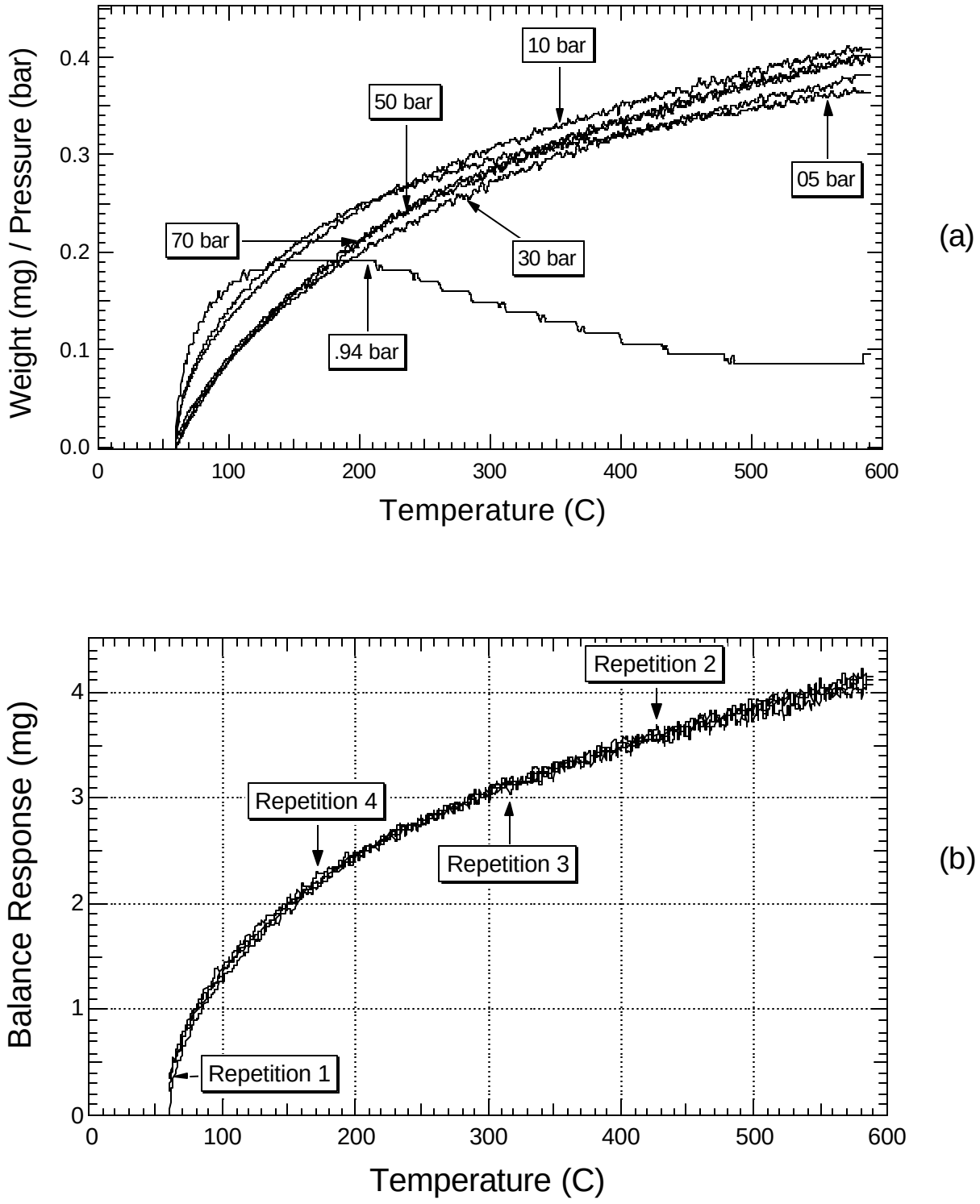

Fig. 6. Data from blank runs: (a) weight of blank run divided by pressure versus temperature and (b) four blank cycles plotted versus temperature.

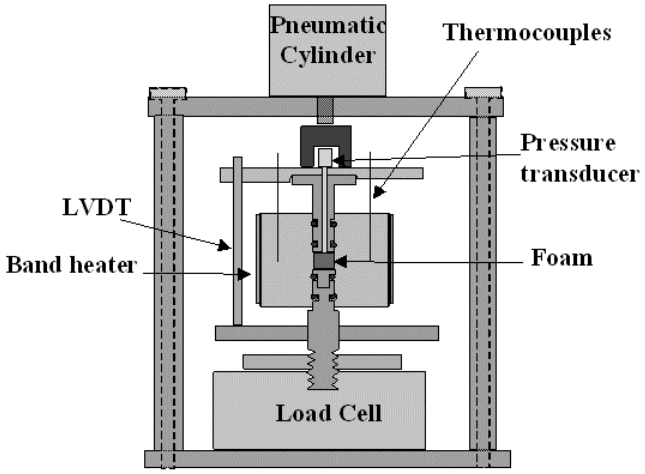

Fig. 7. Schematic diagram of the high-pressure cell experiments.

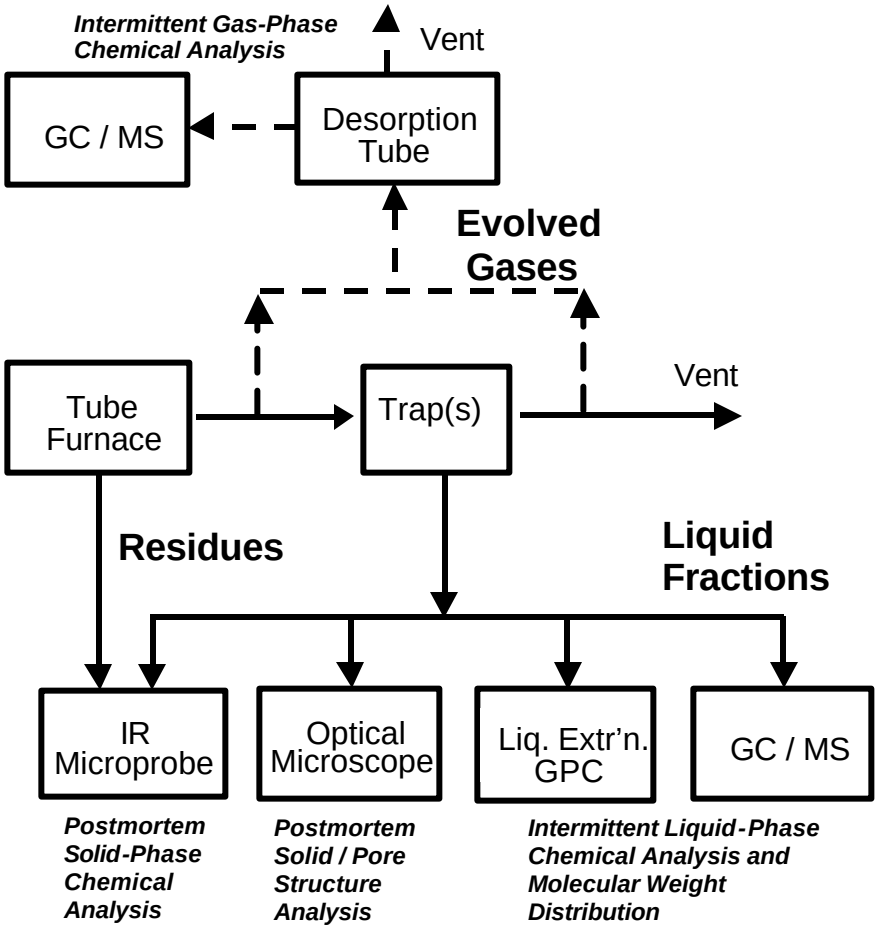

Fig. 8. Schematic diagram of the tube furnace experiments.

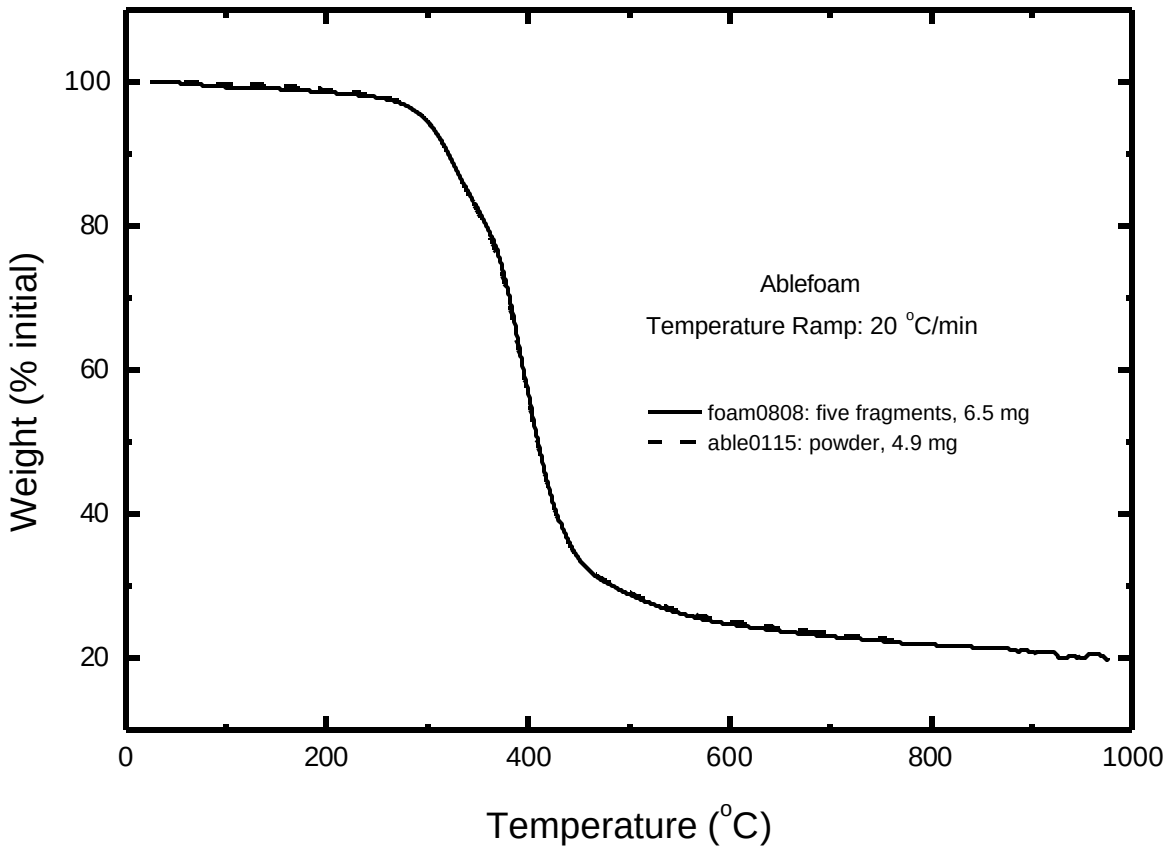

Fig. 9. TGA results (% of initial mass versus time) from constant-heating-rate (20 ^{o}C/min) experiments with two physically different unconfined samples of Ablefoam.

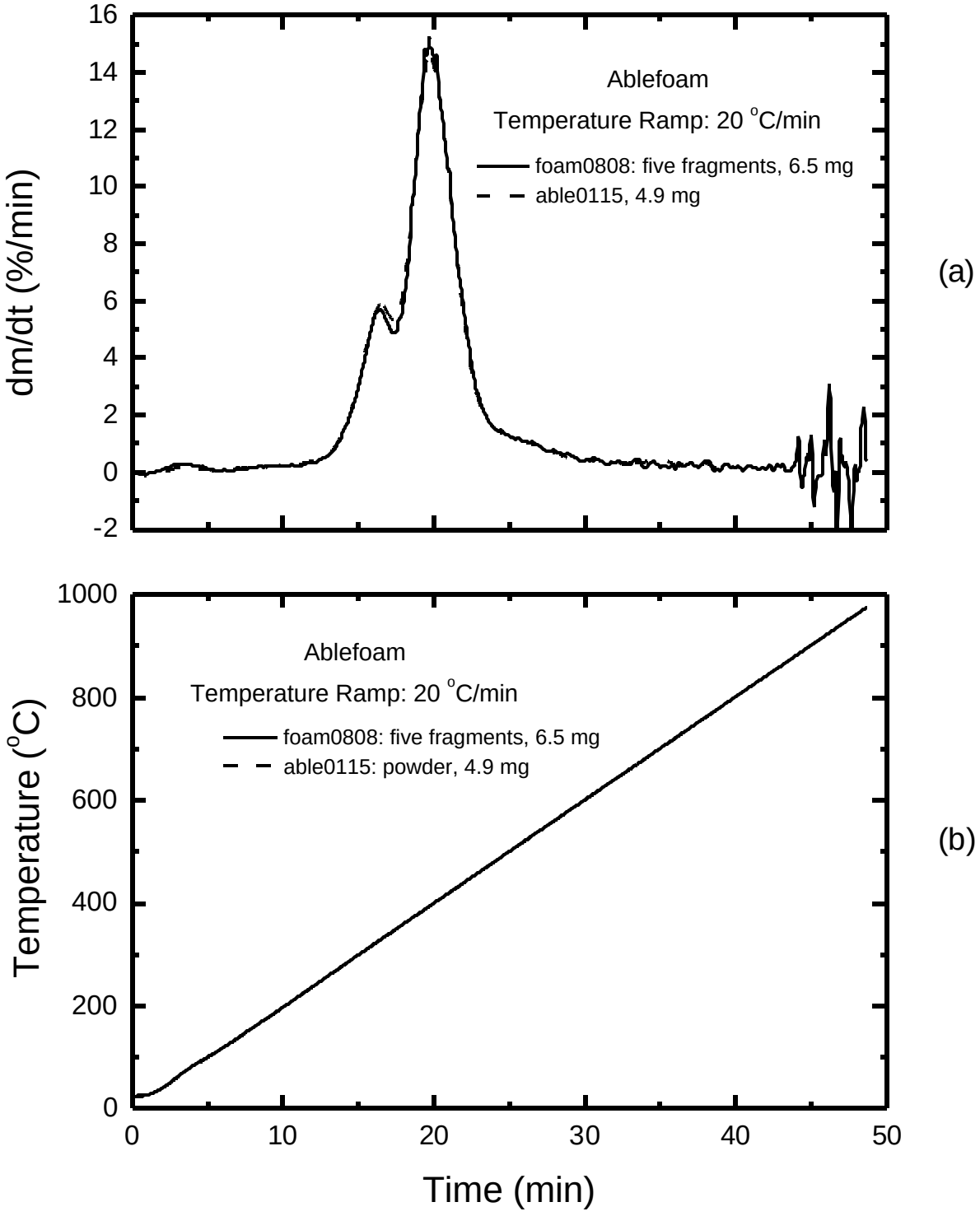

Fig. 10. Rate-of-mass-loss curves (a) and temperature histories (b) corresponding to the TGA results shown in Fig. 9 for the two Ablefoam samples.

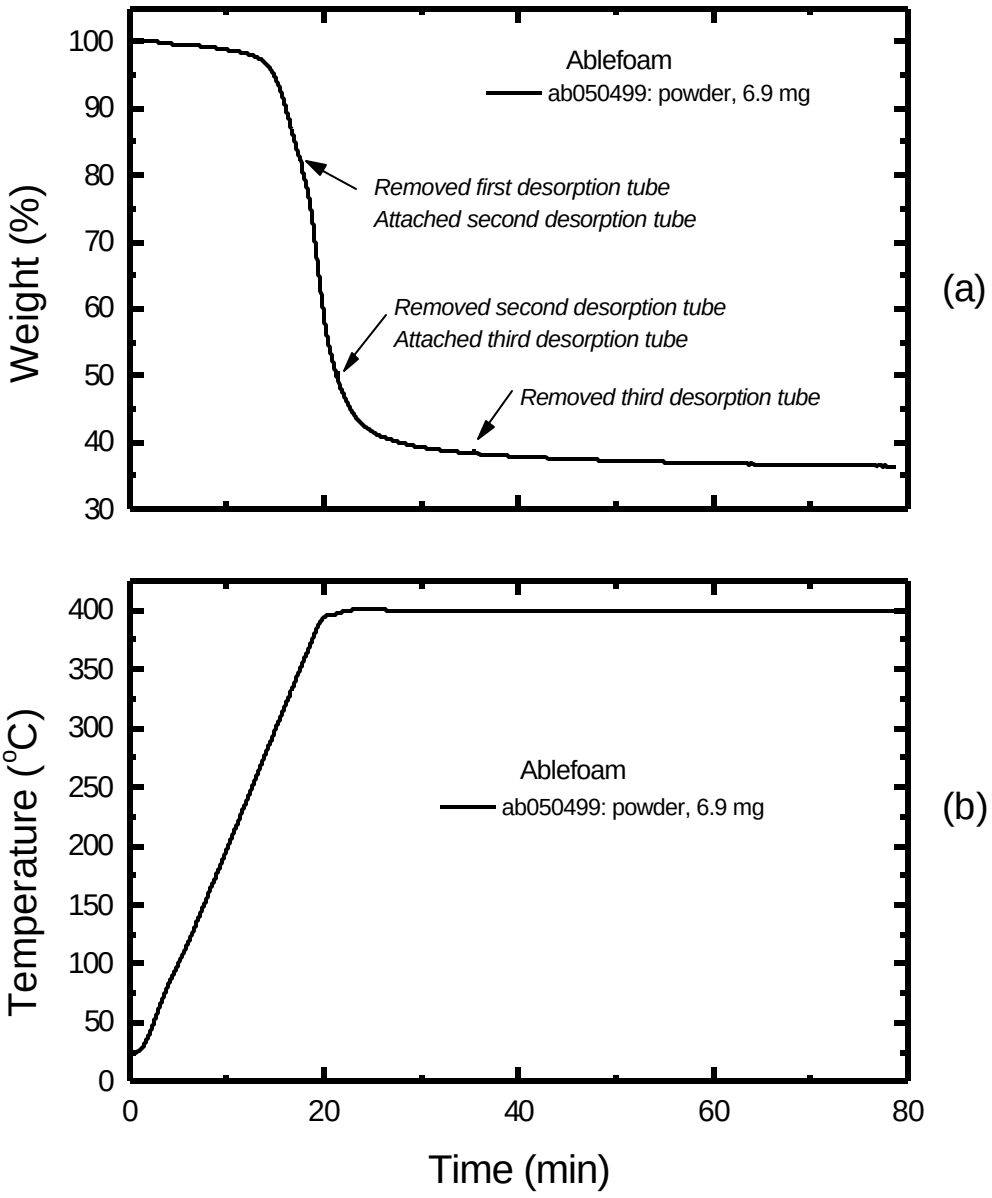

Fig. 11. TGA results (a) and corresponding temperature history (b) from an isothermal (400^{o} C) experiment with a 6.9-mg sample of Ablefoam.

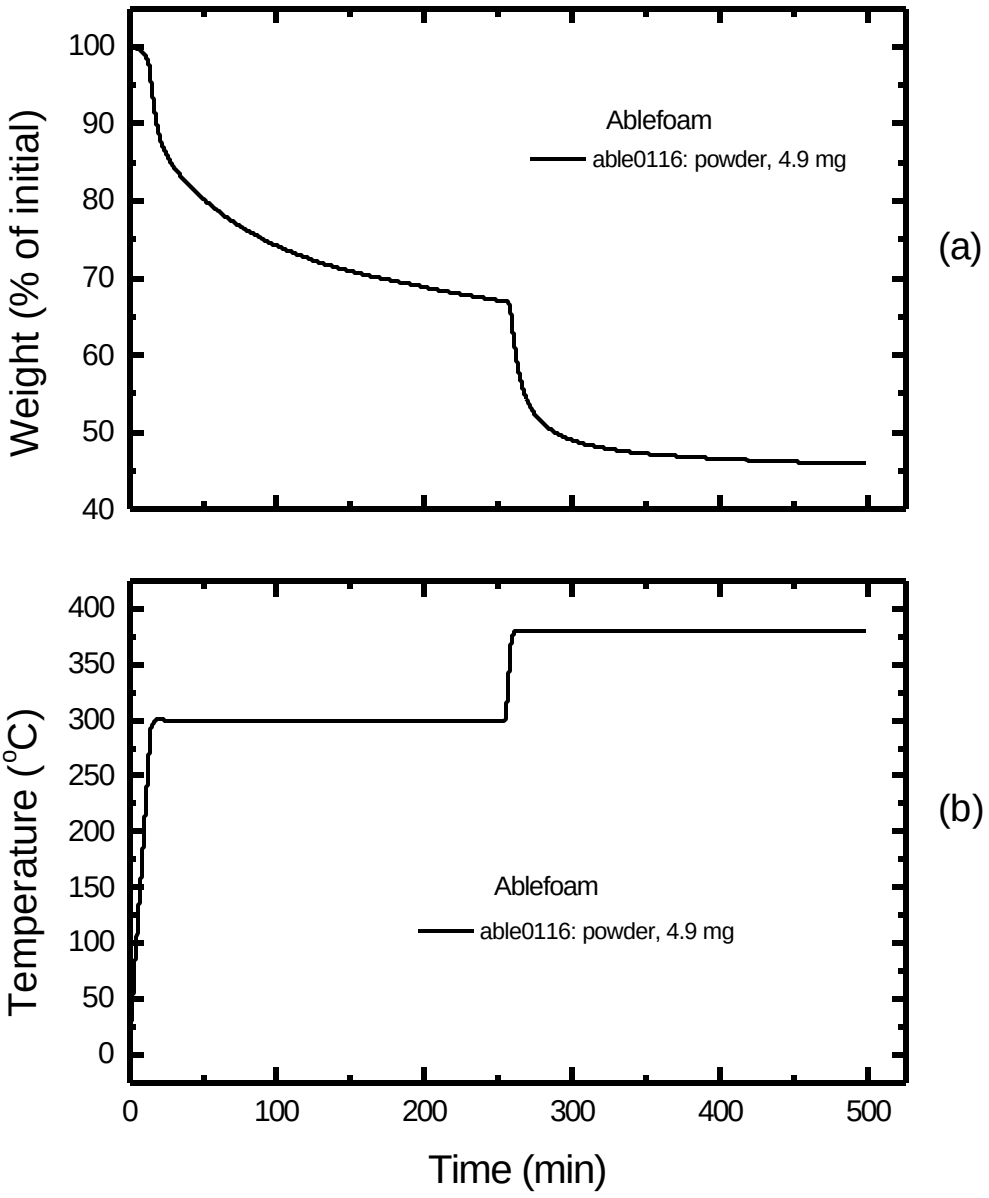

Fig. 12. TGA results (a) and corresponding temperature history (b) from a two-step isothermal (300/380^{o} C) experiment with a 4.9-mg sample of Ablefoam.

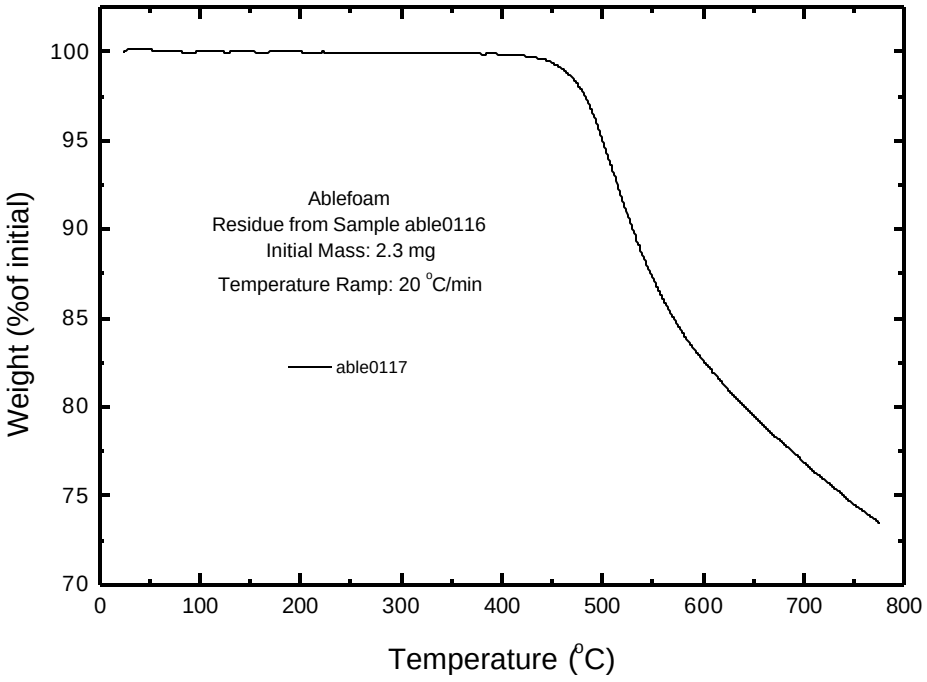

Fig. 13. TGA results (% of initial mass versus time) from constant-heating-rate (20 ^{o}C/min) experiment with the unconfined residue from the two-step isothermal experiment with Ablefoam shown in Fig. 12.

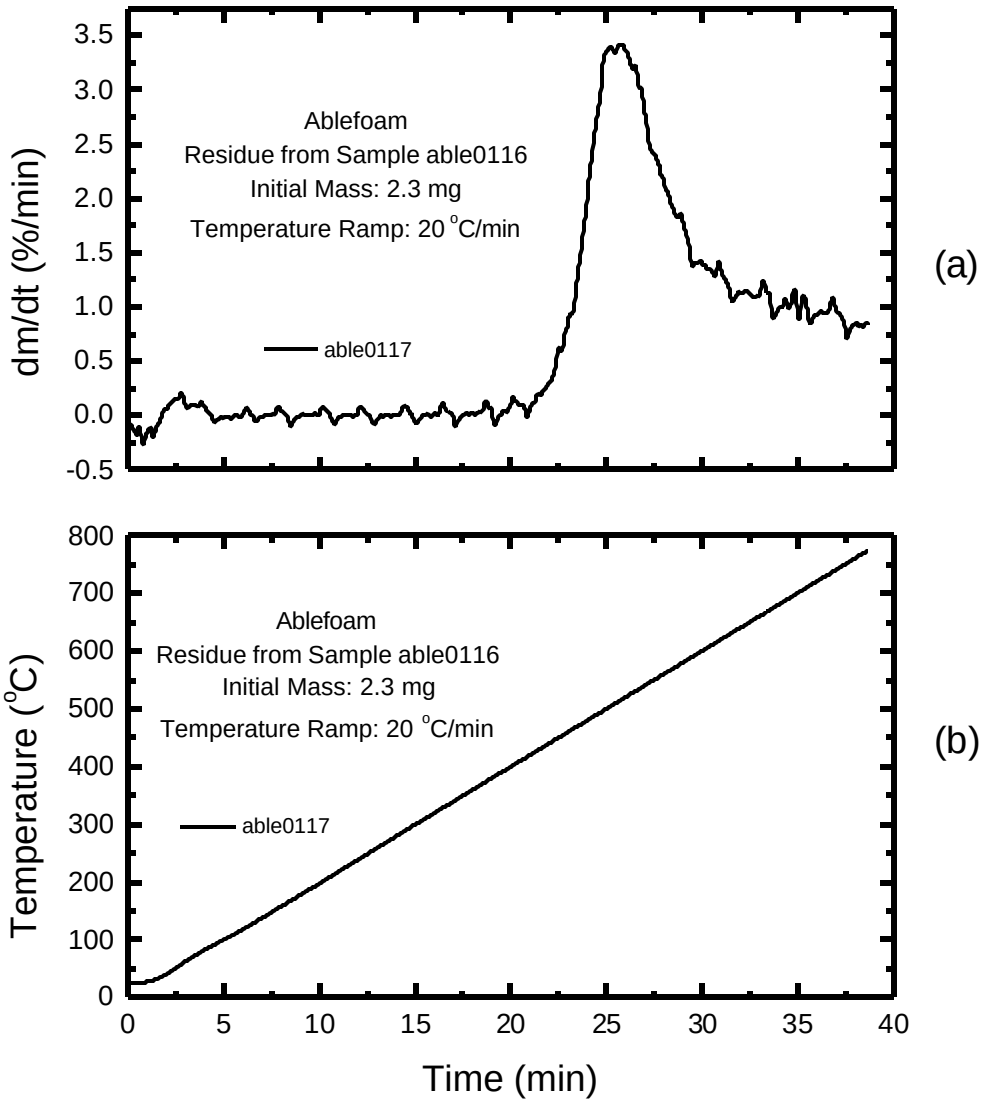

Fig. 14. Rate-of-mass-loss curve (a) and temperature histories (b) corresponding to the TGA results shown in Fig. 13 for the residue from the two-step isothermal experiment with Ablefoam shown in Fig. 12.

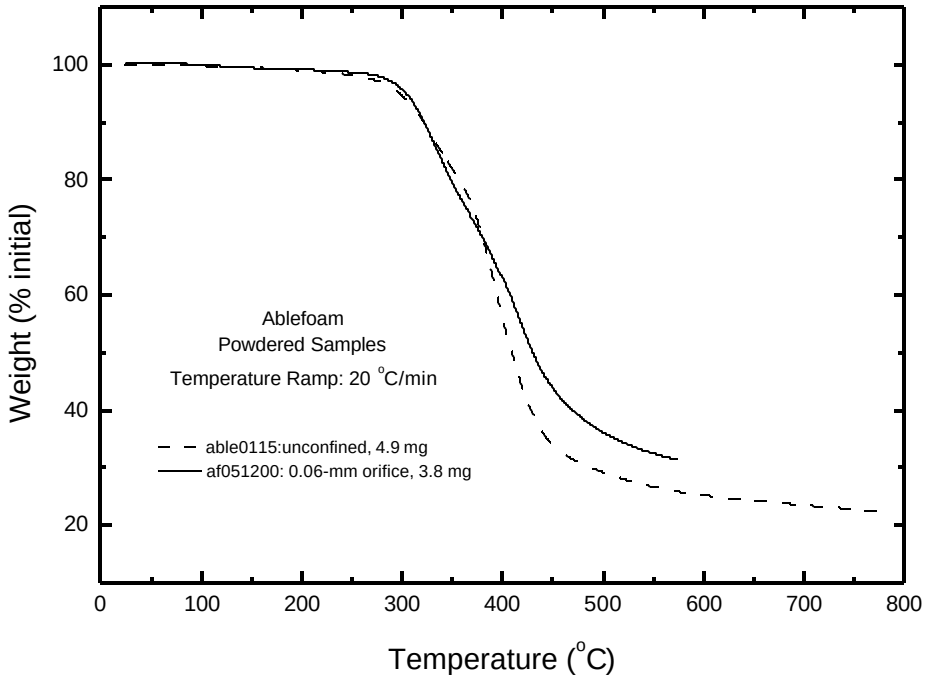

Fig. 15. TGA results (% of initial mass versus time) from constant-heating-rate (20 ^{o}C/min) experiment with a partially-confined (0.06 mm orifice) sample of powdered Ablefoam. The curve from the analogous unconfined sample (Fig. 9) also is shown for comparison.

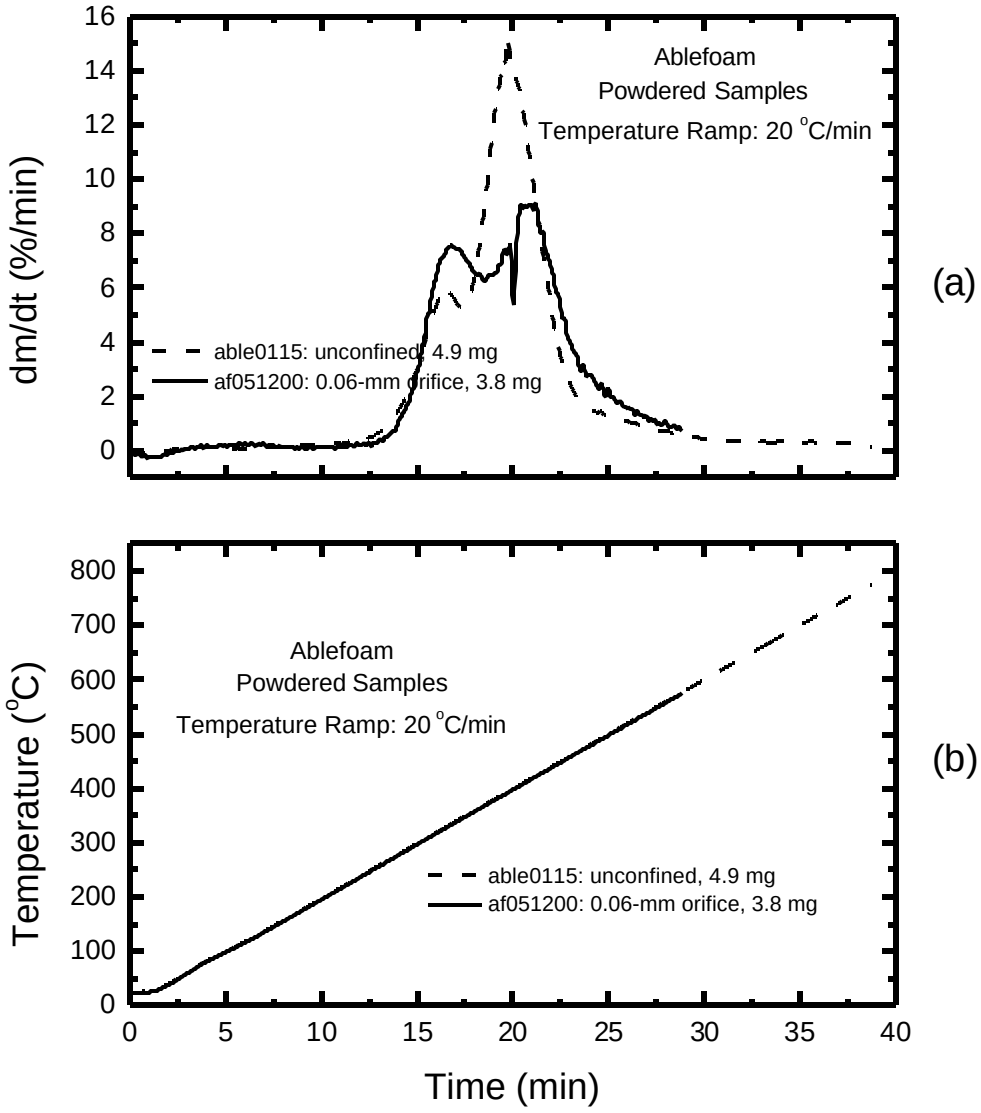

Fig. 16. Rate-of-mass-loss (derivative) curve (a) and temperature history (b) corresponding to the TGA results shown in Fig. 15 for a constant-heating-rate (20 ^{o}C/min) experiment with a partially-confined (0.06 mm orifice) sample of powdered Ablefoam. The curves from the analogous unconfined sample (Fig. 9) also are shown for comparison.

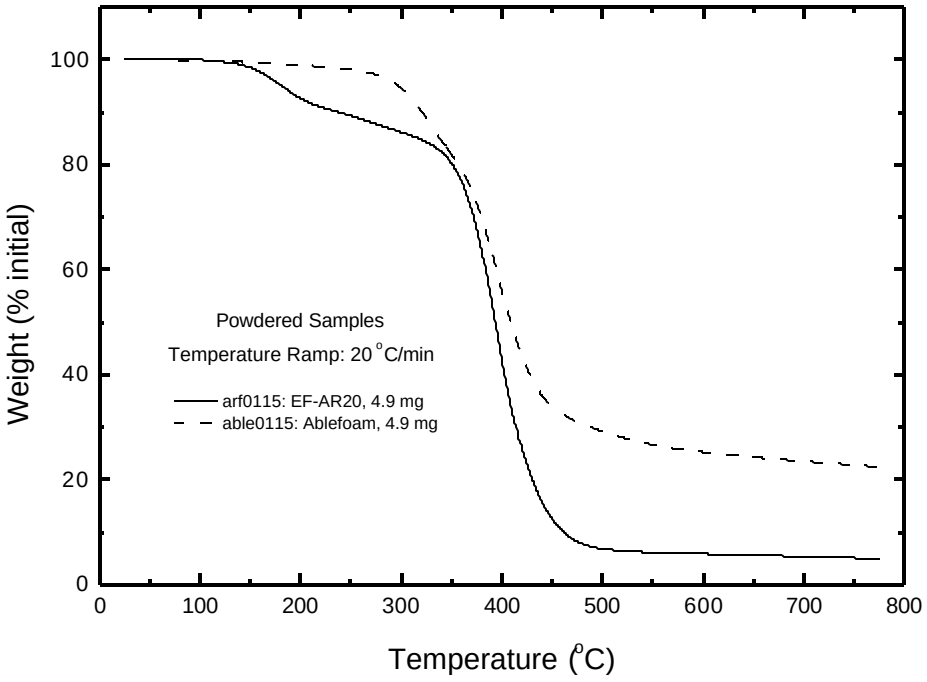

Fig. 17. TGA results (% of initial mass versus time) from constant-heating-rate (20 ^{o}C/min) experiment with an unconfined sample of powdered EF-AR20 foam. The curve from the analogous unconfined sample (Fig. 9) with powdered Ablefoam also is shown for comparison.

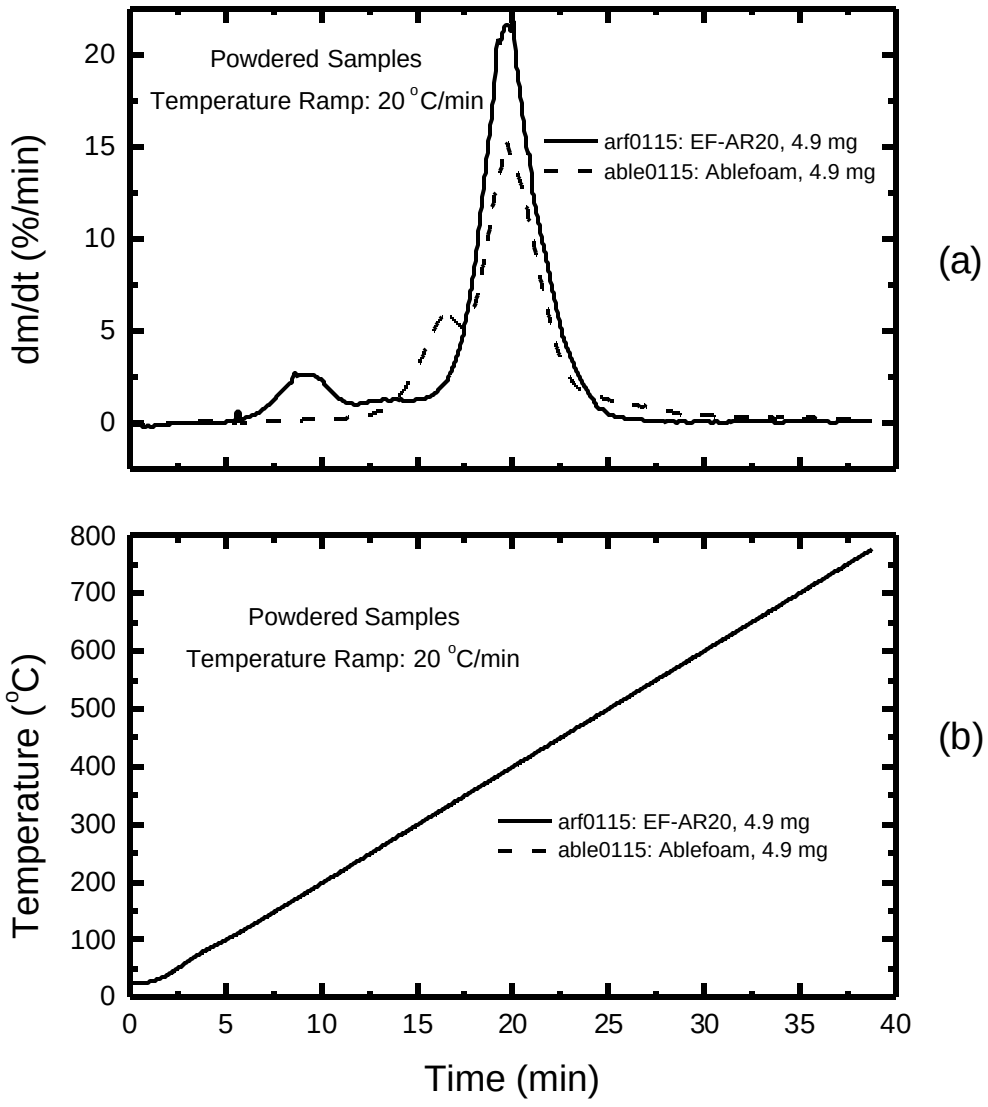

Fig. 18. Rate-of-mass-loss (derivative) curve (a) and temperature history (b) corresponding to the TGA results shown in Fig. 17 for a constant-heating-rate (20 ^{o}C/min) experiment with an unconfined sample of powdered EF-AR20 foam. The curves from the analogous experiment with an unconfined sample powdered Ablefoam (Fig. 9) also are shown for comparison.

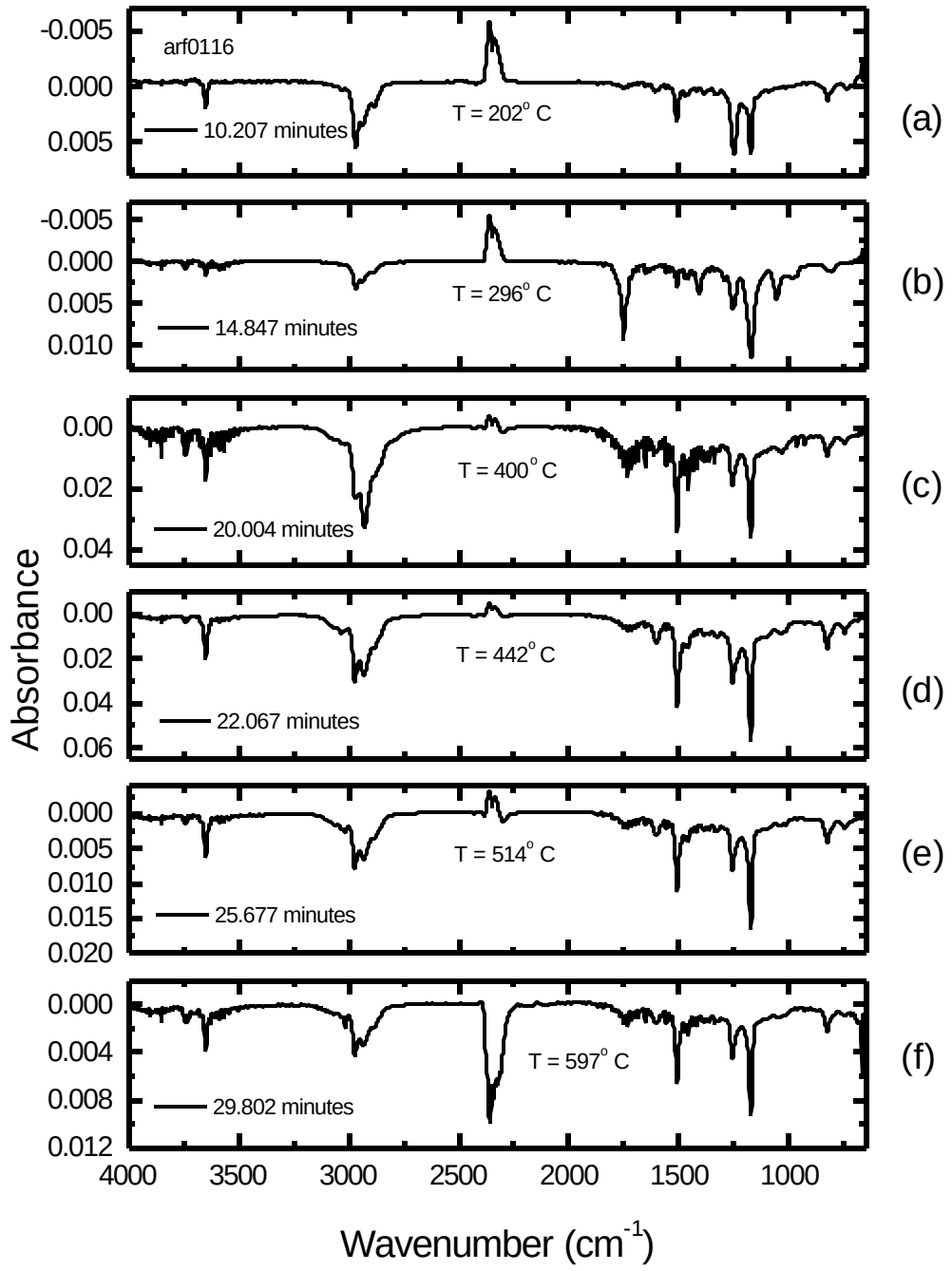

Fig. 19. Selected FTIR spectra that were obtained as a function of time during the conatant-heating-rate (20 ^{o}C/min) TGA experiment (Figs. 17and 18) with an unconfined sample of EF-AR20 foam.

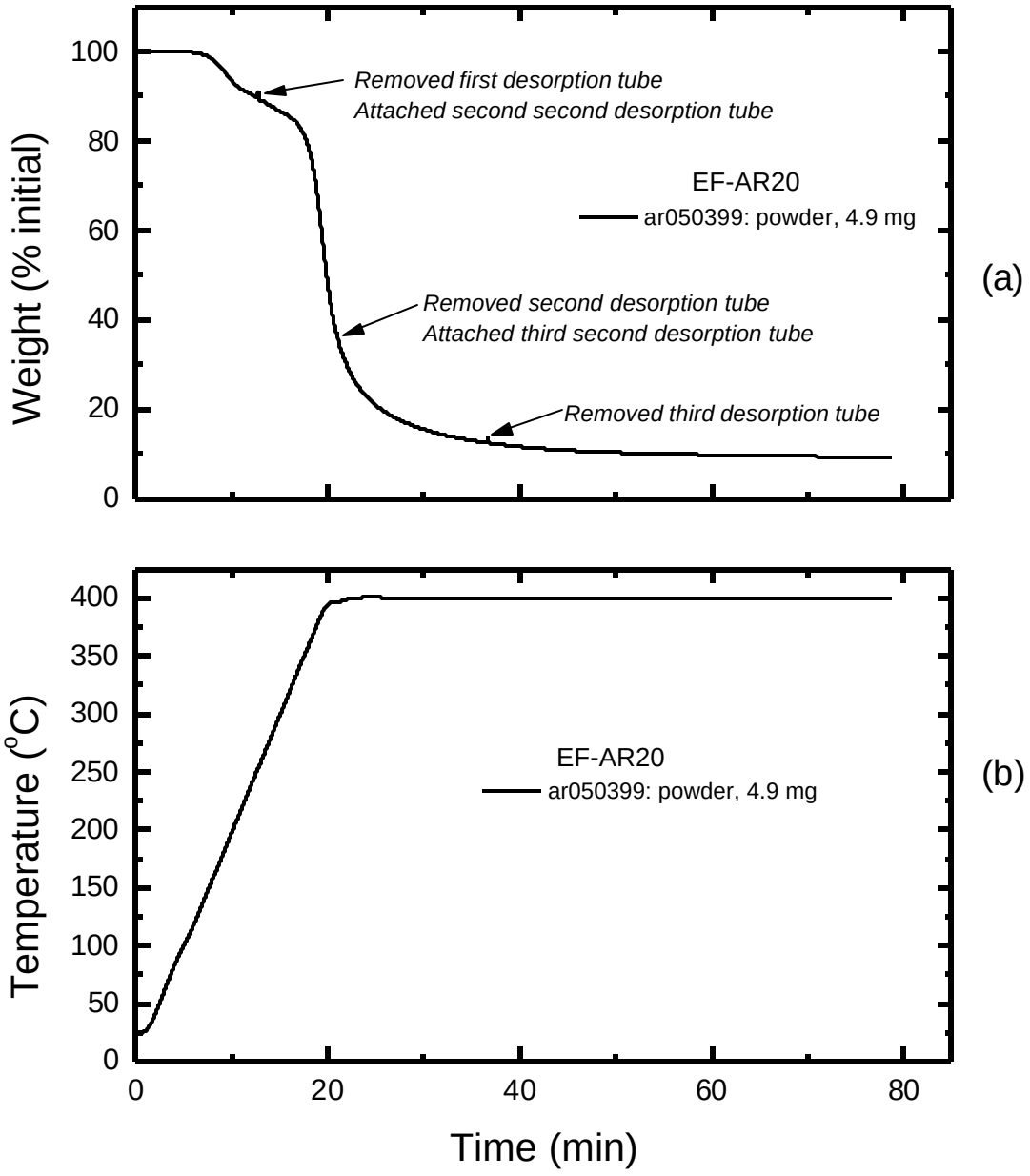

Fig. 20. Mass loss versus time (a) and corresponding temperature history (b) from an isothermal (400^{o} C) TGA experiment with a 4.9-mg sample of EF-AR20 foam.

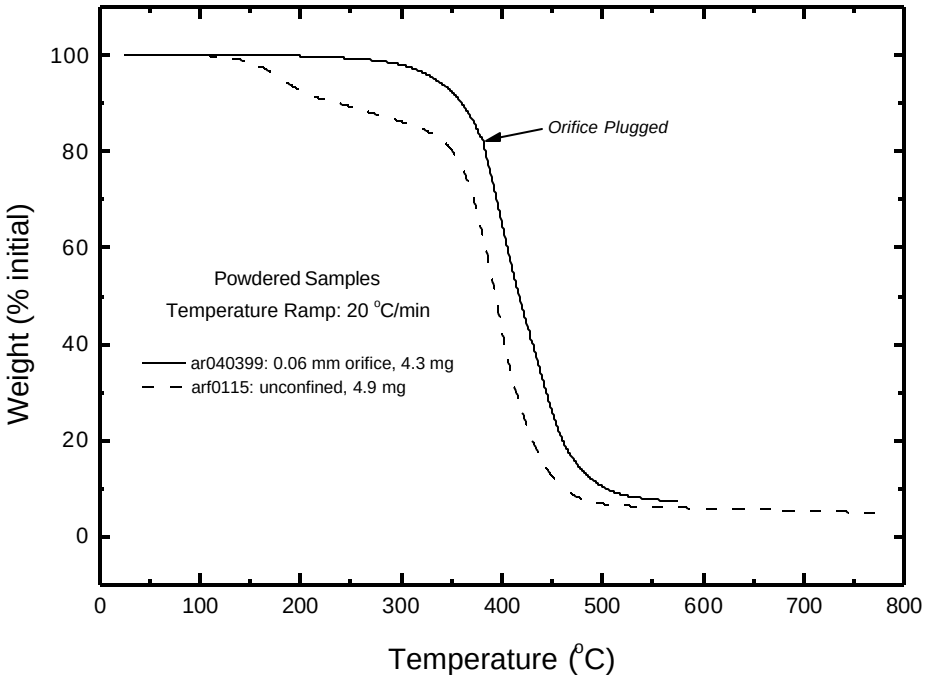

Fig. 21. TGA results (% of initial mass versus time) from constant-heating-rate (20 ^{o}C/min) experiment with a partially-confined (0.06 mm orifice) sample of powdered Ef-AR20. The curve from the analogous unconfined sample (Fig. 17) also is shown for comparison.

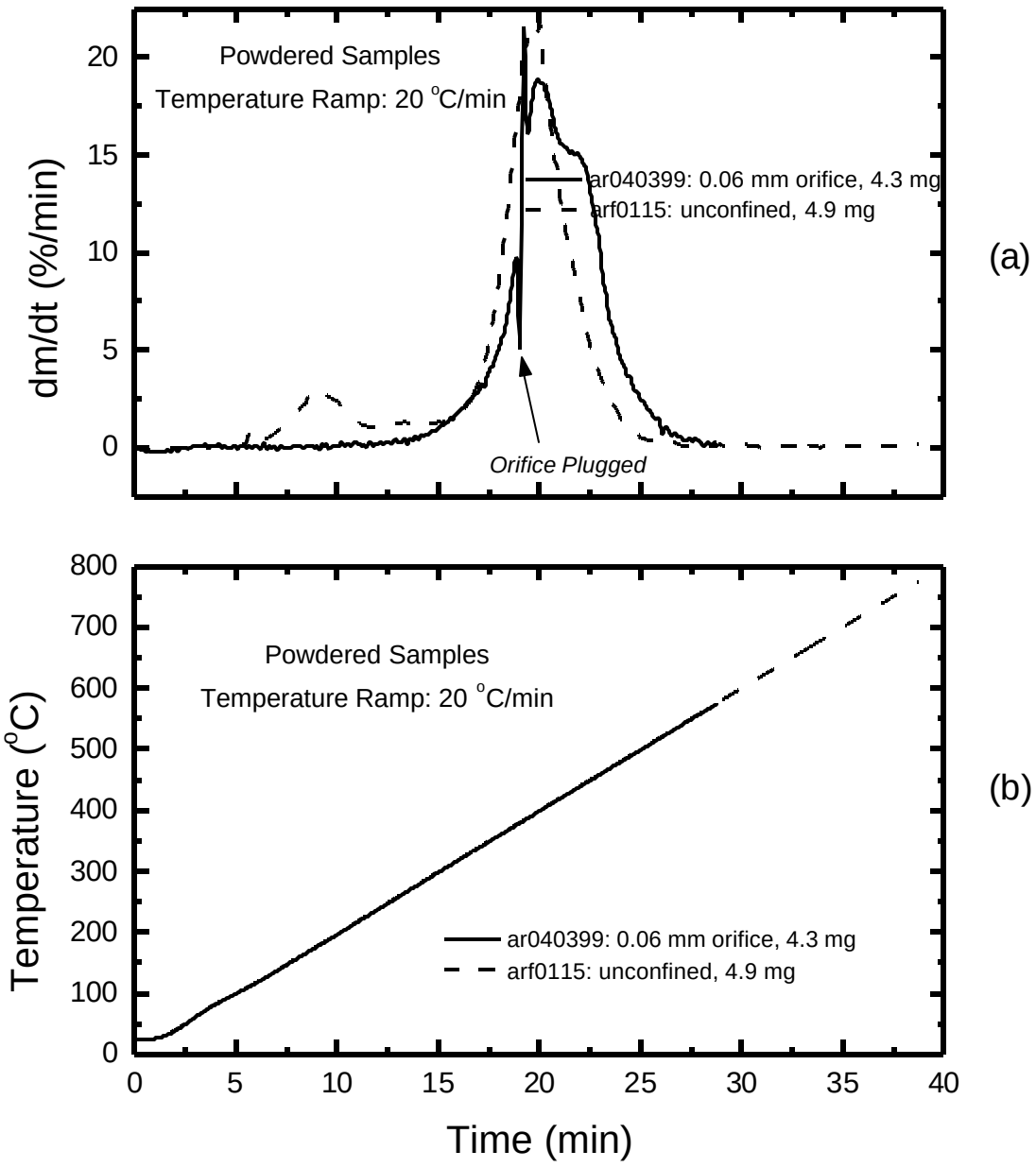

Fig. 22. Rate-of-mass-loss (derivative) curve (a) and temperature history (b) corresponding to the TGA results shown in Fig. 21 for a constant-heating-rate (20 °C/min) experiment with a partially-confined (0.06-mm orifice) sample of powdered EF-AR20 foam. The curves from the analogous experiment with an unconfined sample of powdered Ef-AR20 foam (Fig. 17) also are shown for comparison.

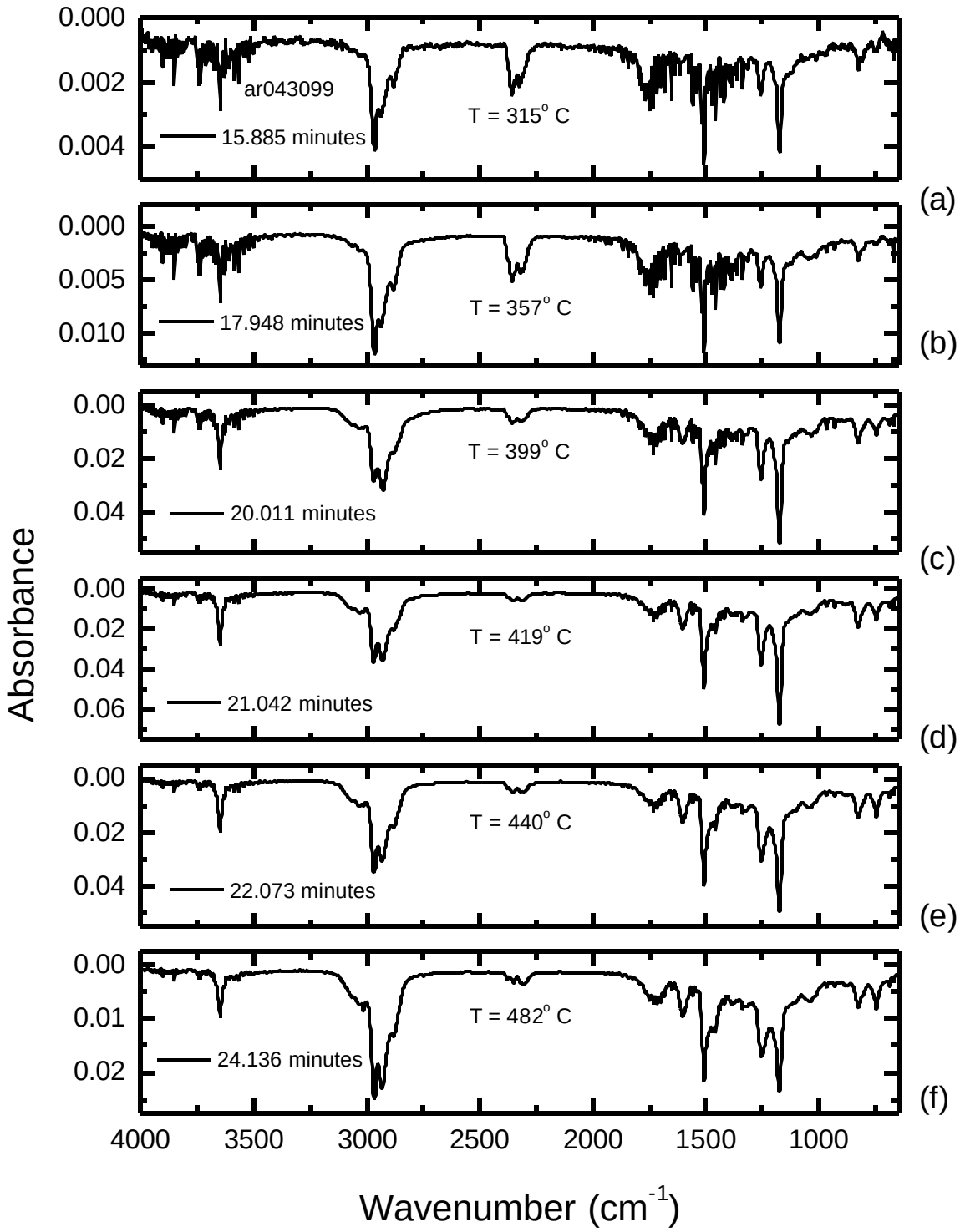

Fig. 23. Selected FTIR spectra that were obtained as a function of time during the conatant-heating-rate (20 ^{o}C/min) TGA experiment (Figs. 21and 22) with a partially-confined (0.06-mm orifice) sample of EF-AR20 foam.

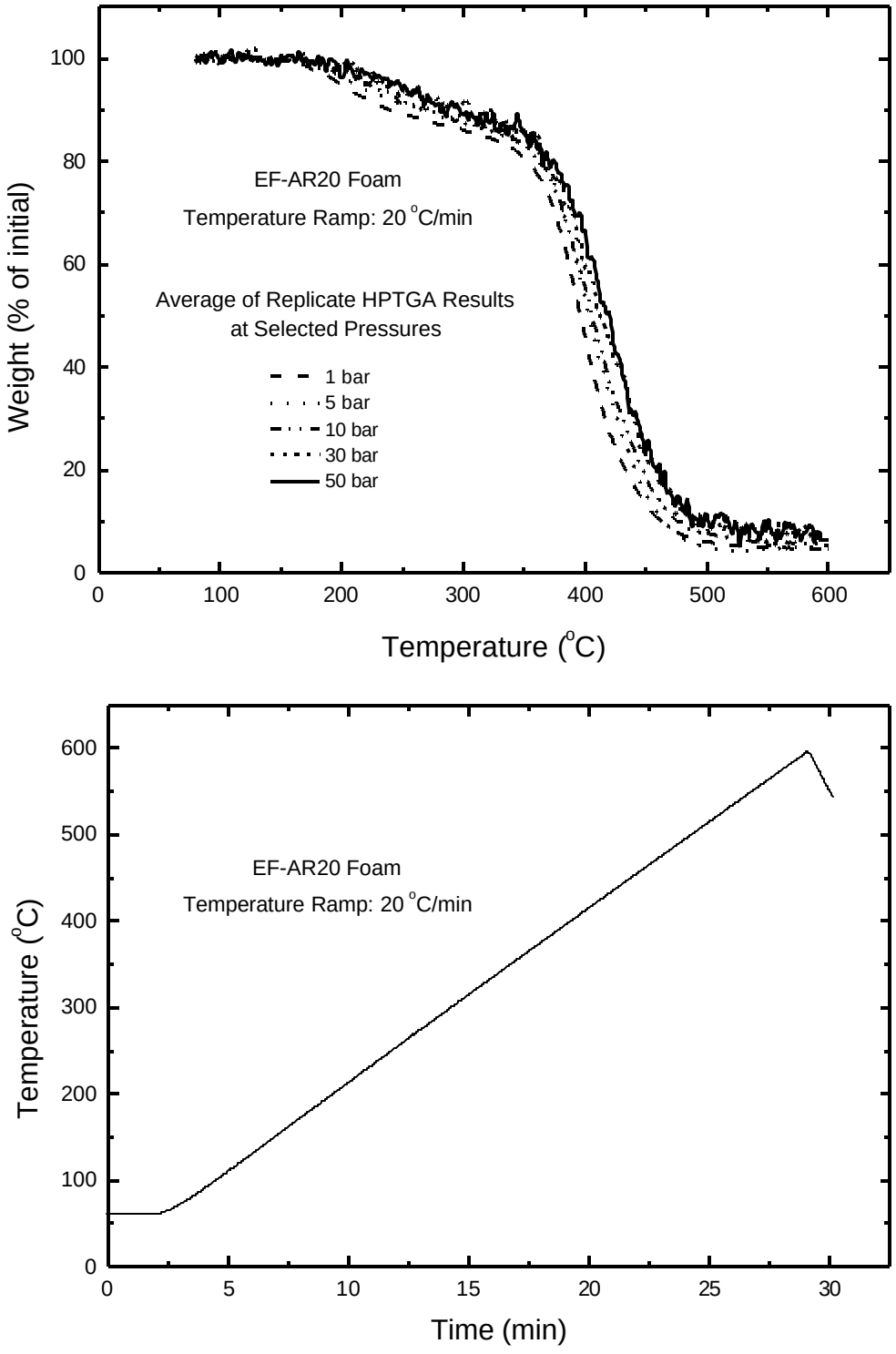

Fig.24. HPTGA results: (a) average percent of initial mass versus time and (b) average temperature history from constant-heating-rate (20 ^{o}C/min) experiment with unconfined samples Ef-AR20.

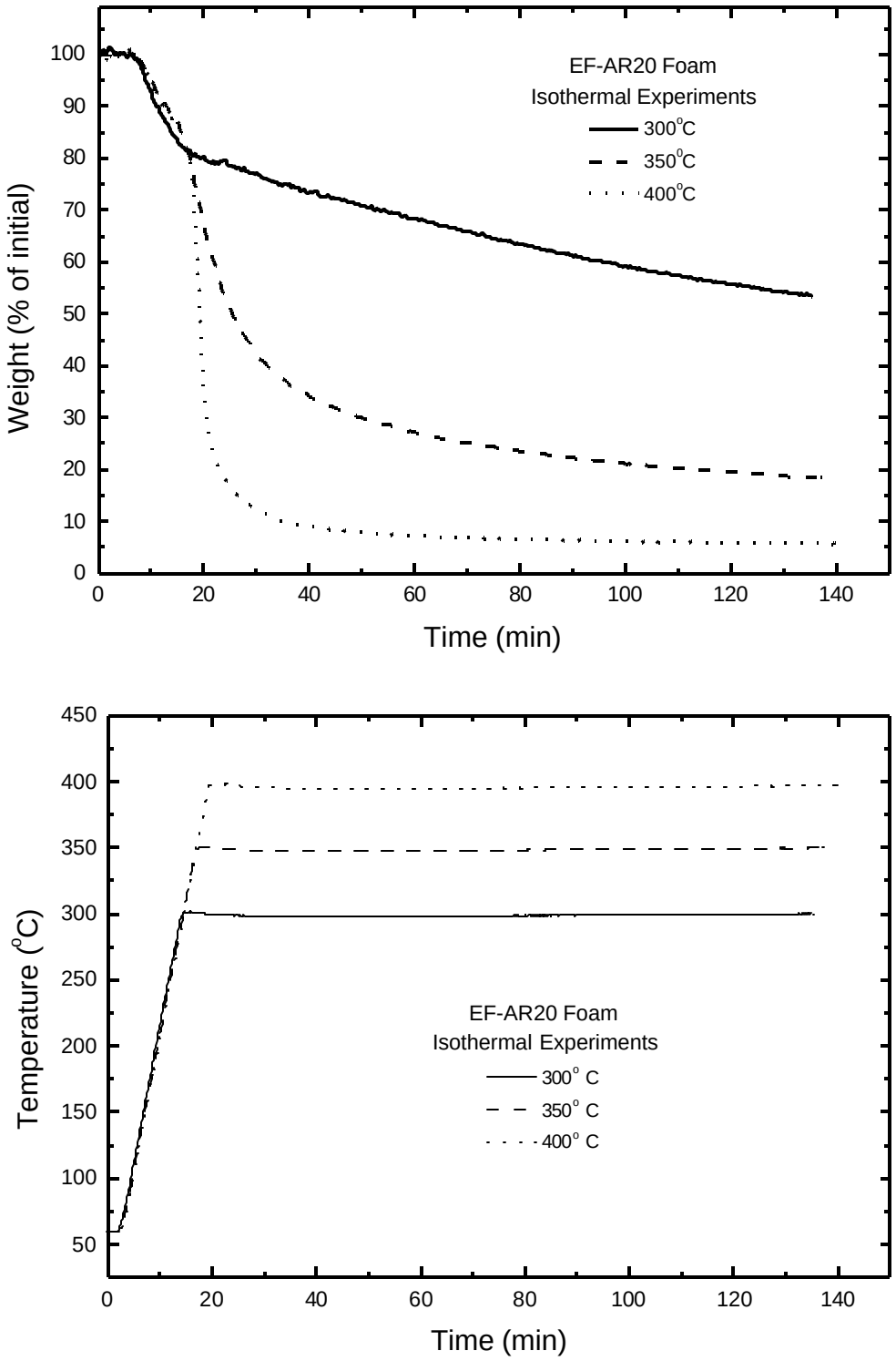

Fig. 25. HPTGA results at 1 bar pressure: (a) average percent of initial mass versus time and (b) average temperature history from isothermal experiments with unconfined samples of EF-AR20.

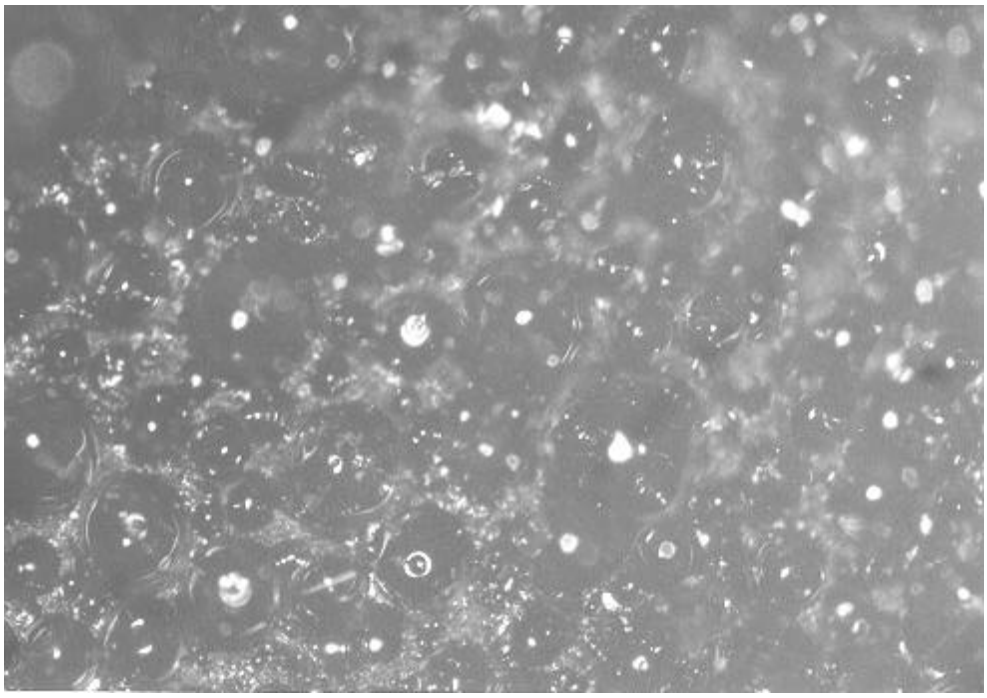

(a)

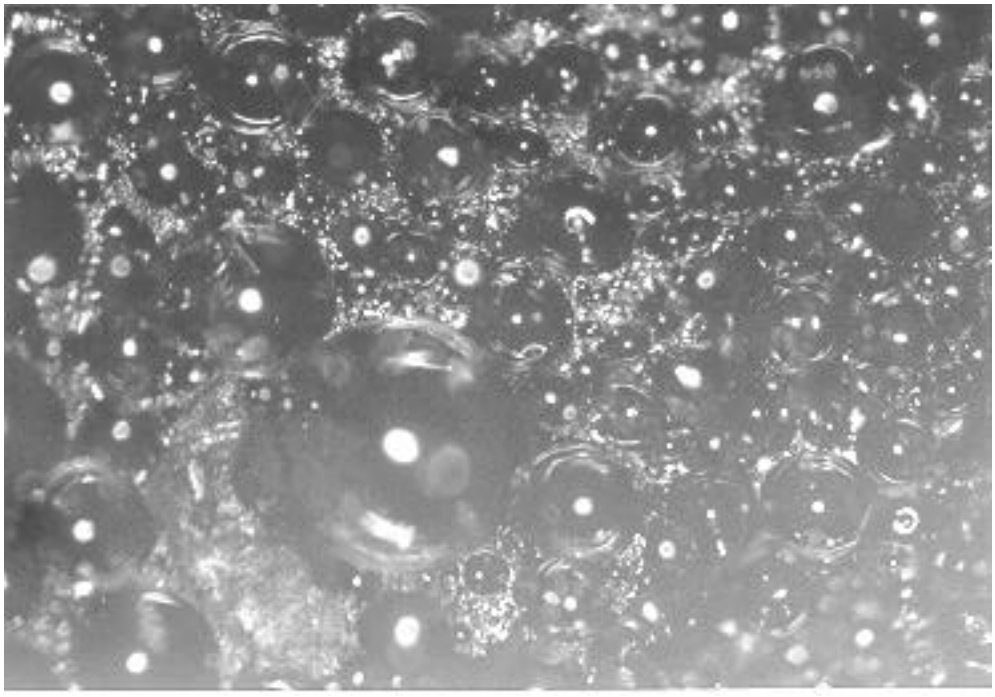

(b)

.

Fig. 26. Micrographs (about 30x) of EF-AR20 foam samples after heating at 20 ^{o}C/min to: (a) 300^{o} C and (b) 350^{o} C.

.

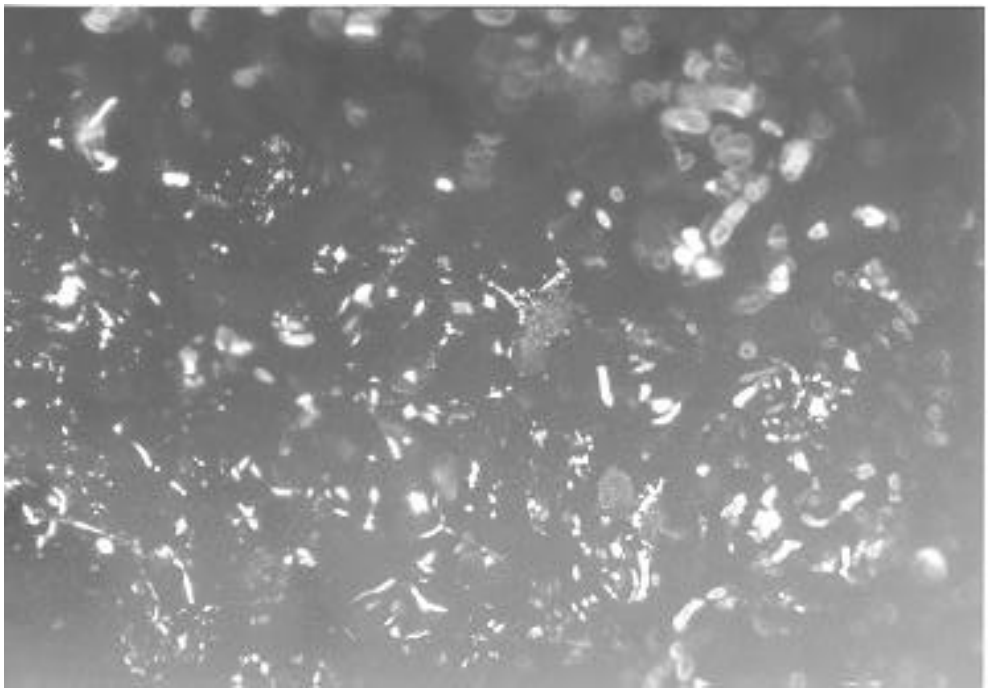

(a)

(b)

.Fig. 27. Micrographs (about 30x) from two EF-AR20 foam samples after heating at 20 ^{o}C/min to 400^{o} C: (a) sample showing incipient liquefaction and (b) sample that liquefied.

Fig. 28. Micrographs (about 30x) from EF-AR20 foam sample after heating at 20 ^{o}C/min to 450^{o} C: obvious liquefaction.

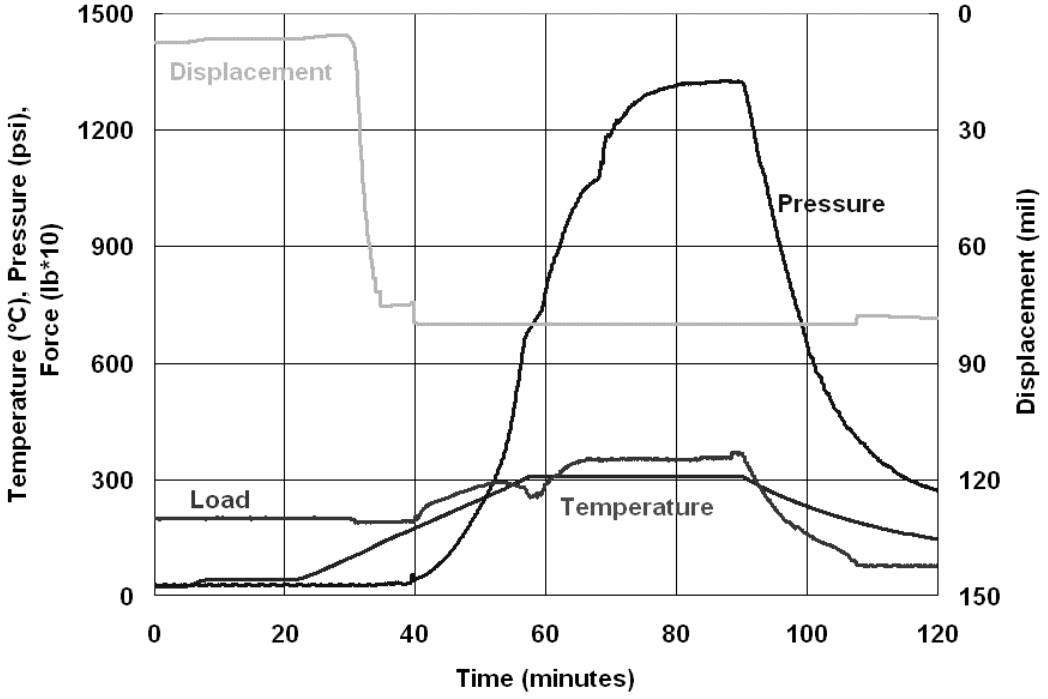

Fig. 29. Results from high-pressure cell experiment with Ablefoam.

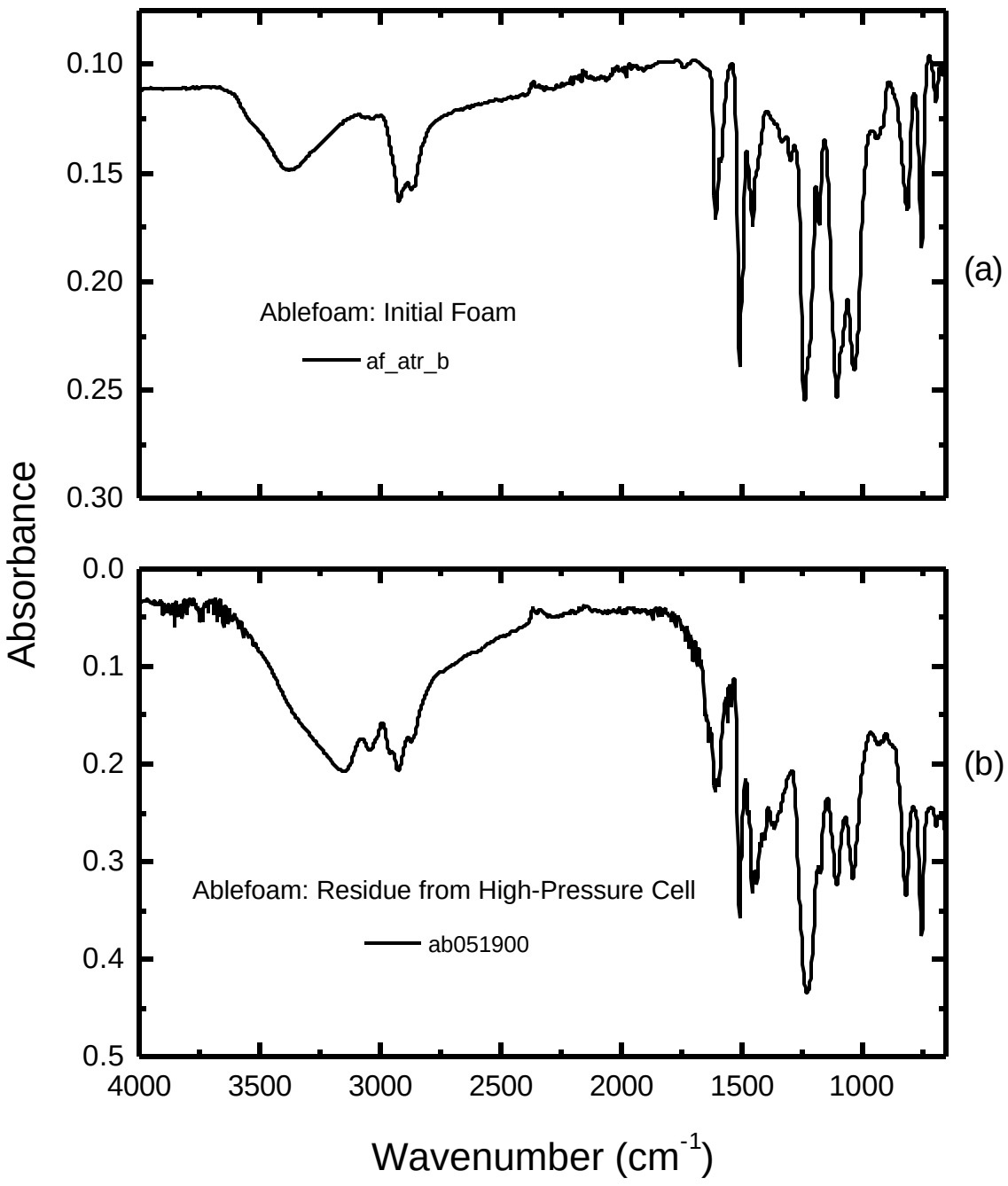

Fig. 30. IRMP spectra (a) from residue formed in high-pressure cell experiment with Ablefoam and (b) from initial Ablefoam.

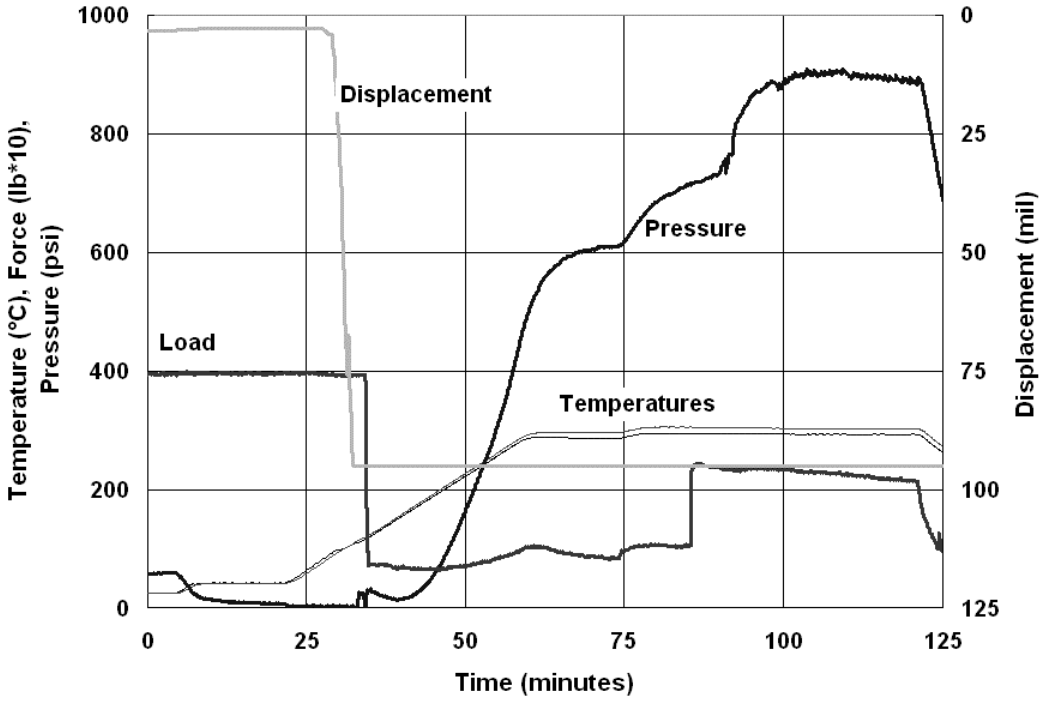

Fig. 31. Results from high-pressure cell experiment with EF-AR20.

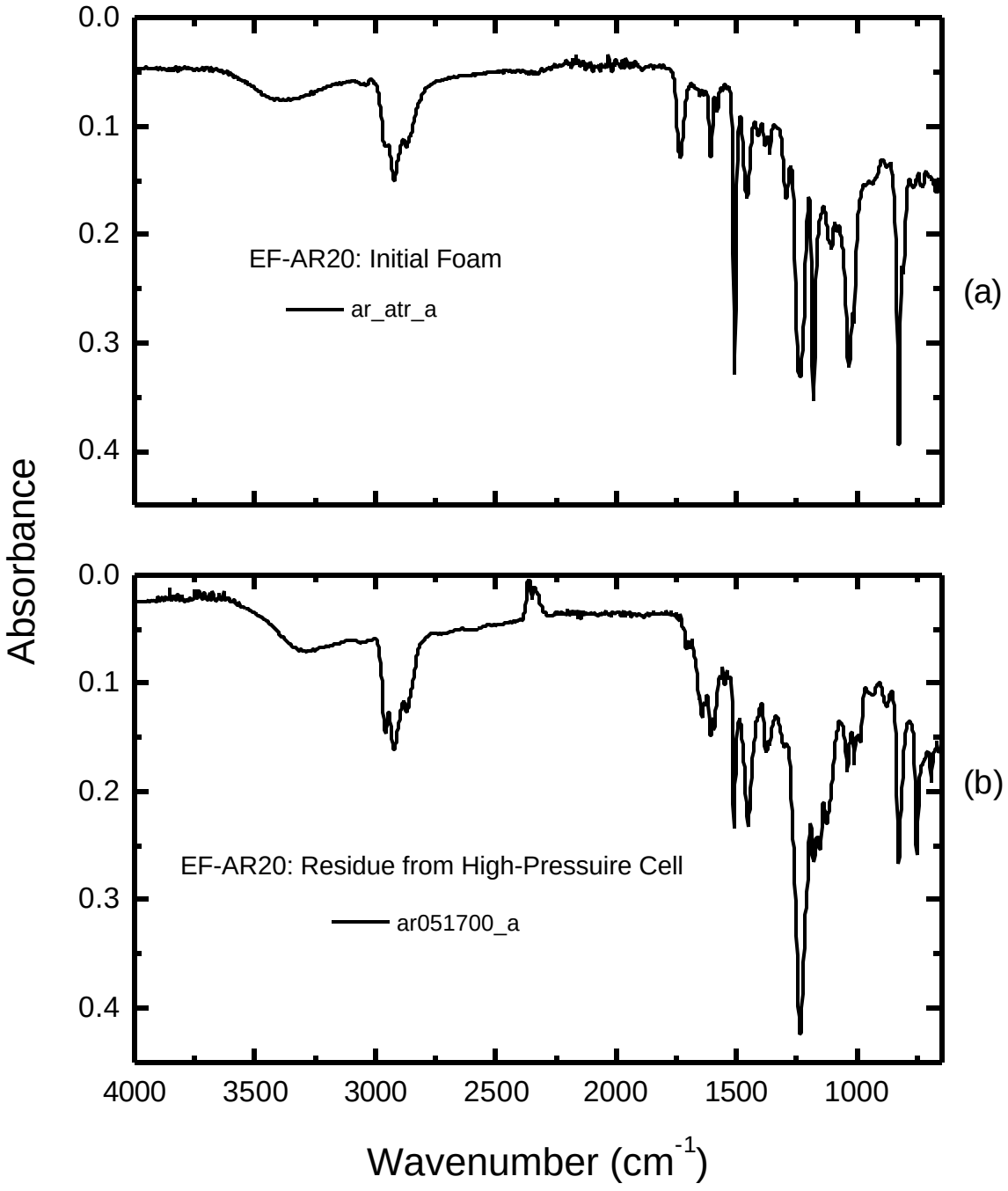

Fig. 32. IRMP spectra (a) from residue formed in high-pressure cell experiment with EF-AR20 foam and (b) from initial EF-AR20 foam

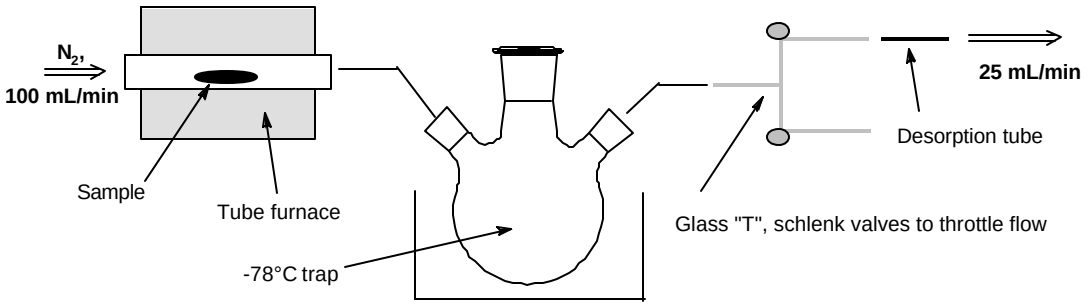

Fig. 33a. Tube furnace pyrolysis apparatus for desorption tube gas sample collection.

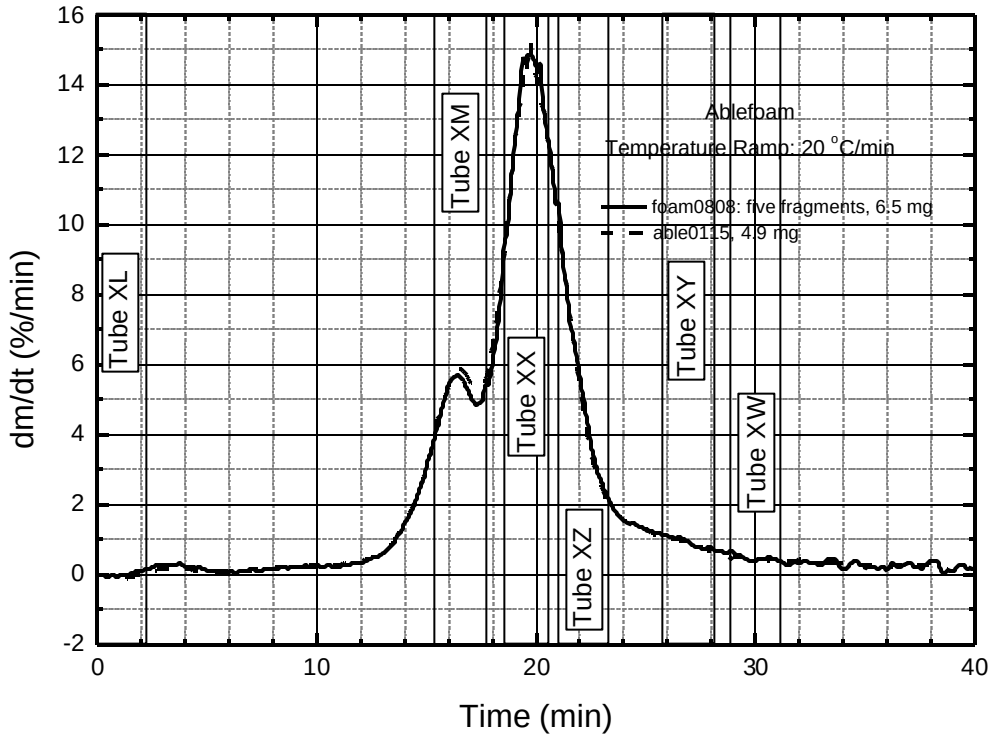

Fig. 33b. Desorption tube sample points for GC-MS analysis of Ablefoam based on TGA data profile.

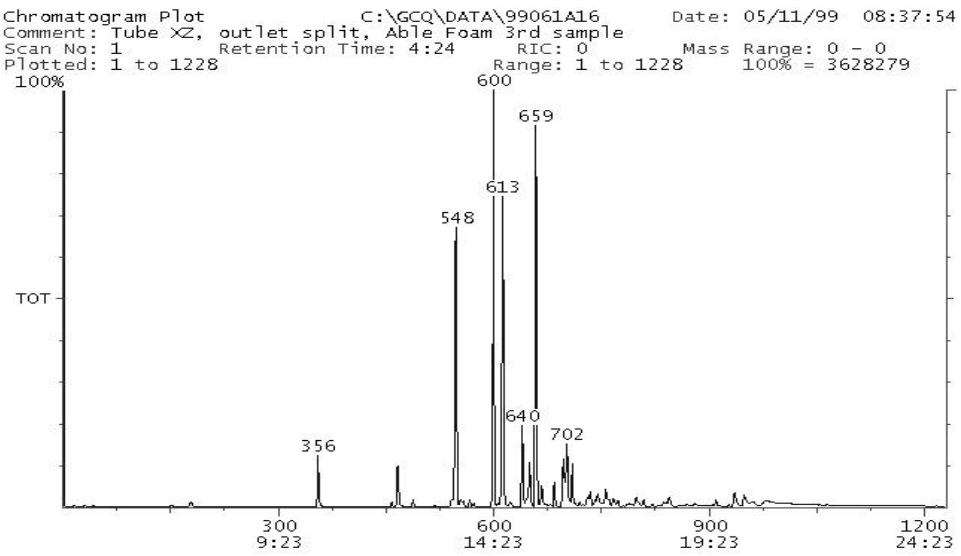

Fig. 34a. Total Ion Chromatogram (TIC) for tube XZ from Ablefoam pyrolysis.

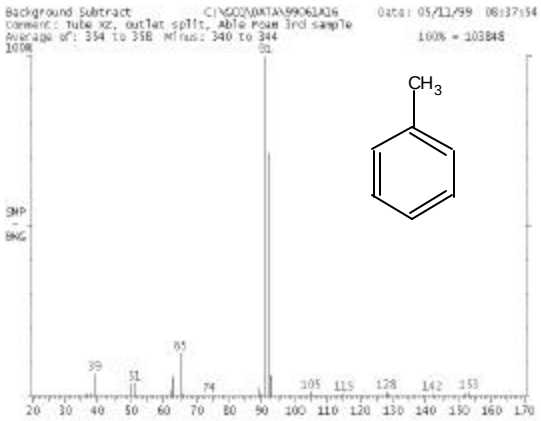

Figure 34b. Toluene at scan 356

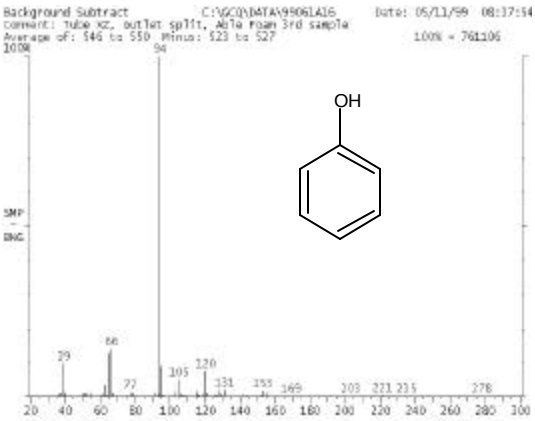

Figure 34c. Phenol at scan 548

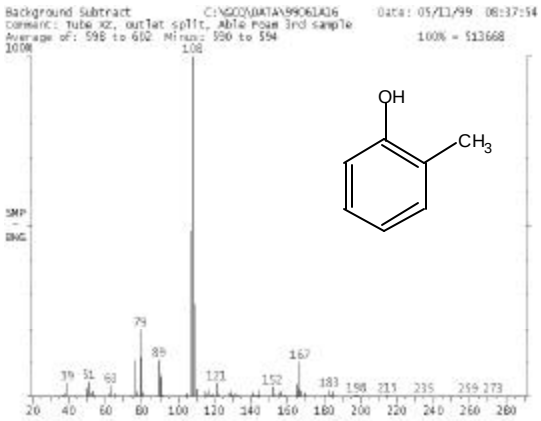

Figure 14d. o-Cresol at scan 600

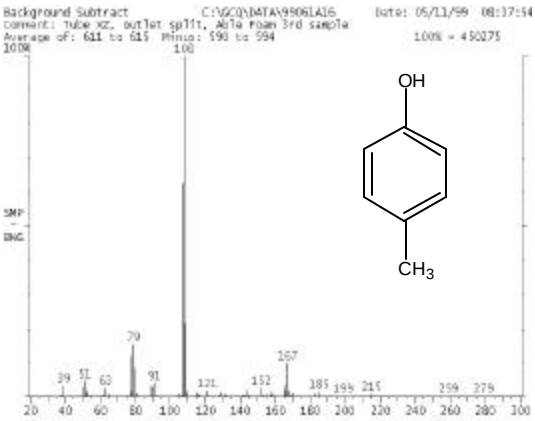

Figure 32e. p-Cresol at scan 613

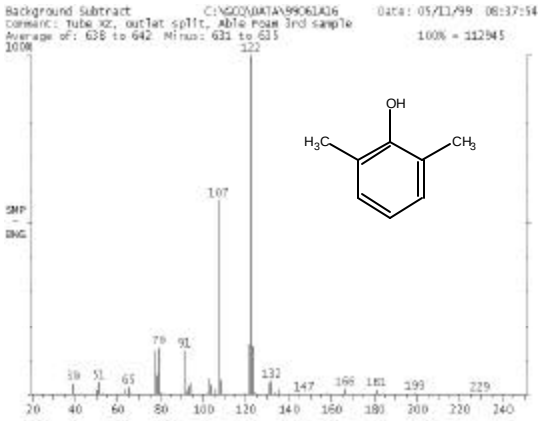

Figure 34f. 2,6-Dimethylphenol at scan 640

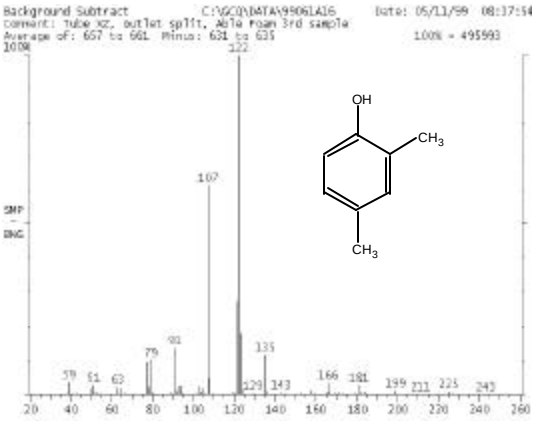

Figure 34g. 2,4-Dimethylphenol at scan 659

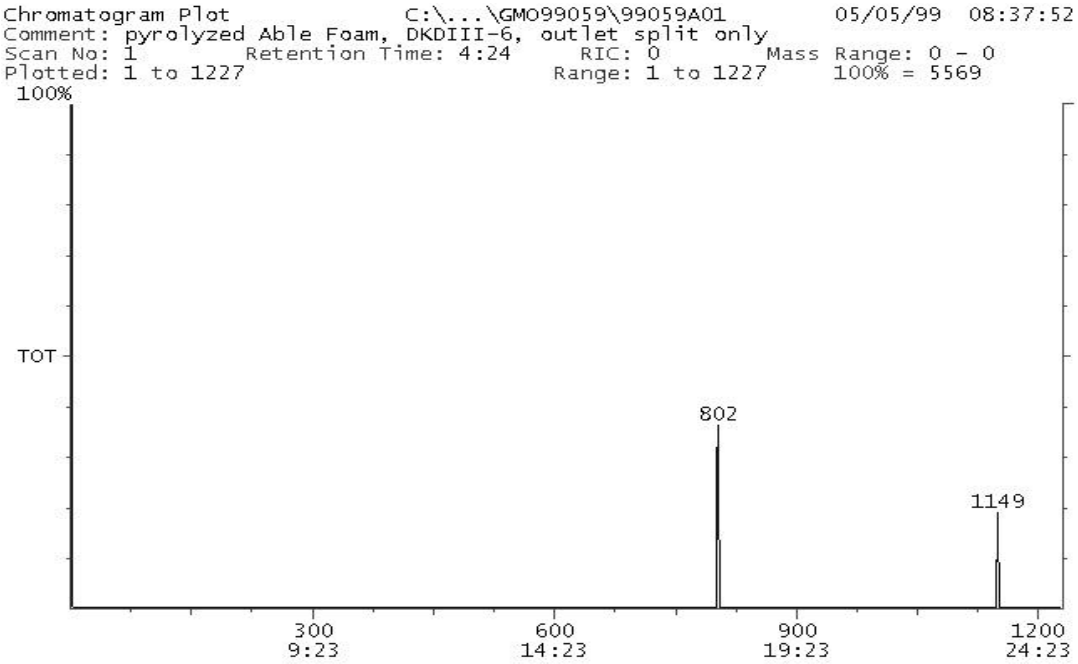

Fig. 35. Total ion chromatogram (TIC) from pyrolyzed Ablefoam.

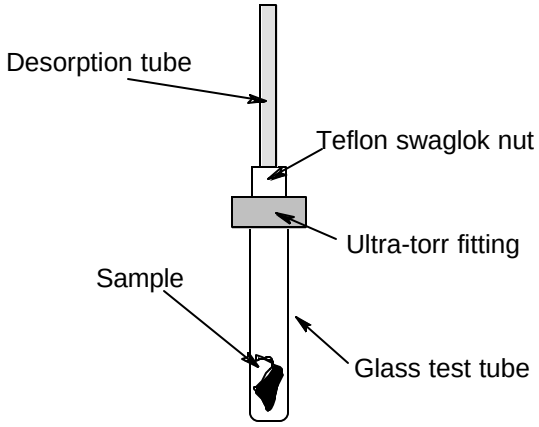

Fig. 36. Passive headspace sampling fixture for GC-MS analysis of pyrolyzed Ablefoam.

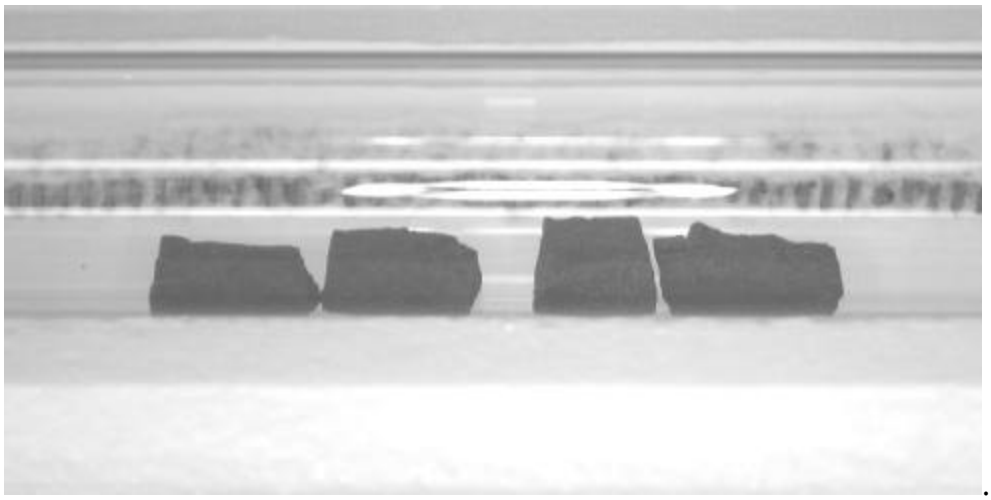

Fig. 37. Ablefoam pieces in quartz tube.

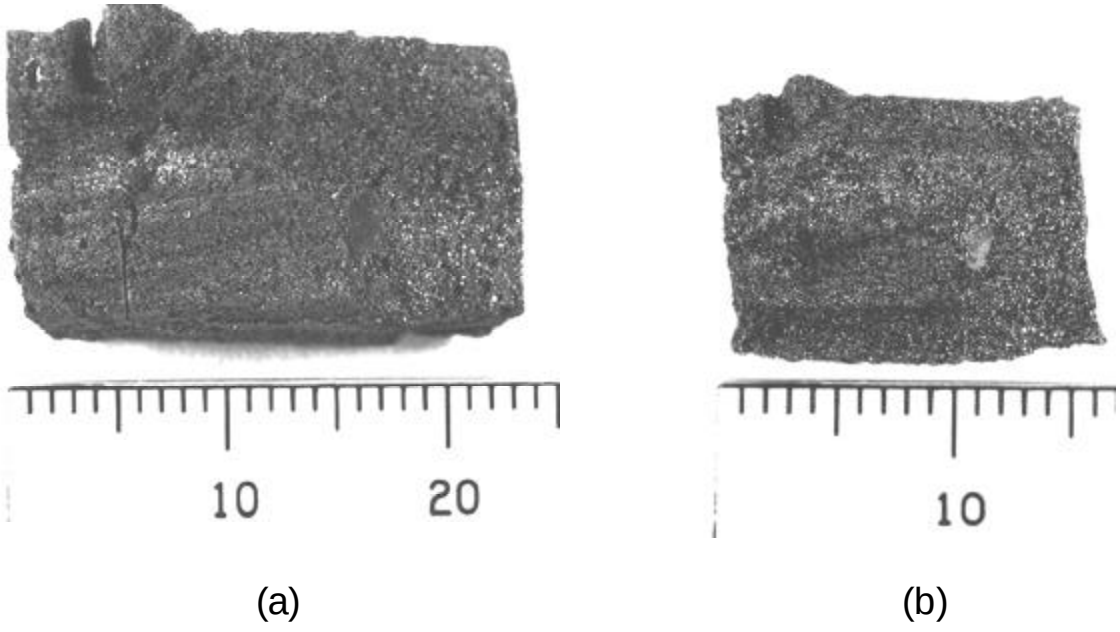

Fig. 38. Optical microscopy images of (a) Ablefoam piece before heating and (b) Ablefoam piece after 600^{o} C bake for 4 hours.

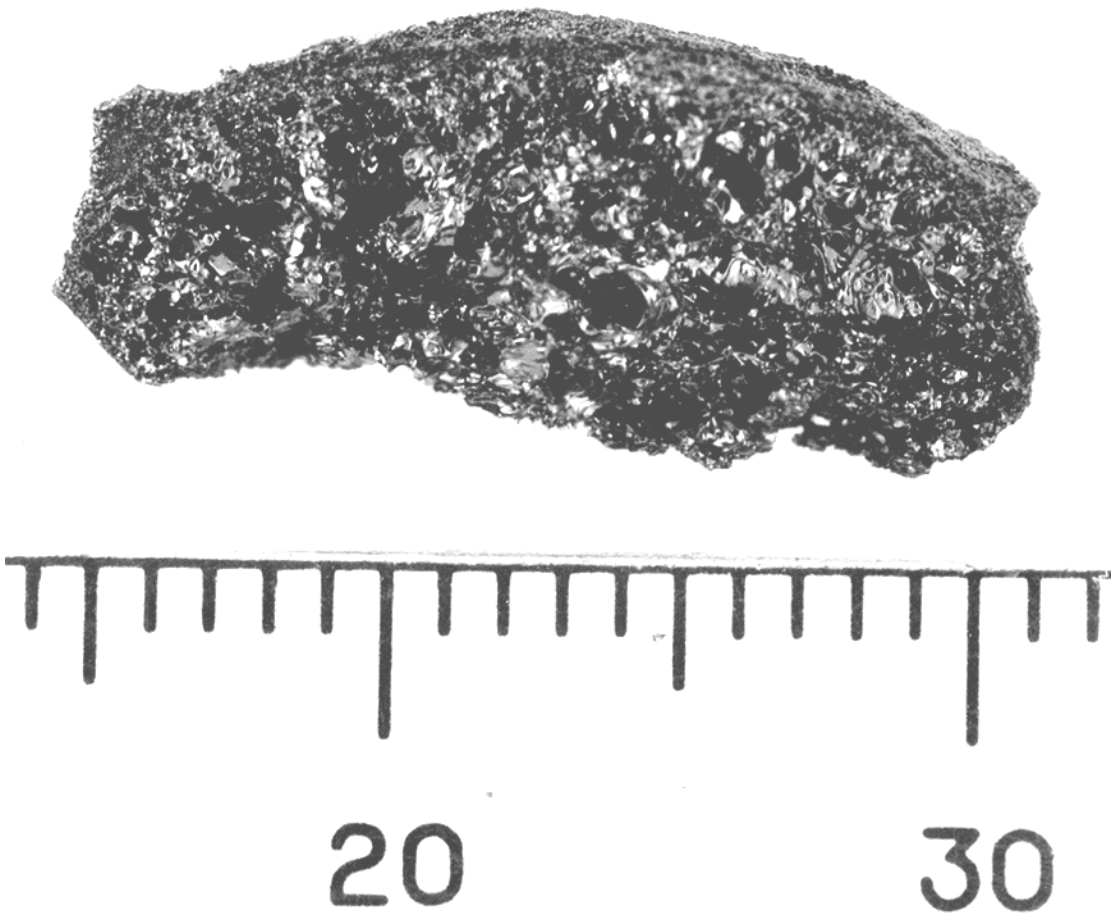

Fig. 39. Optical microscopy 5-x image of Ablefoam fracture surface after 600^{o} C bake for 4 hours.

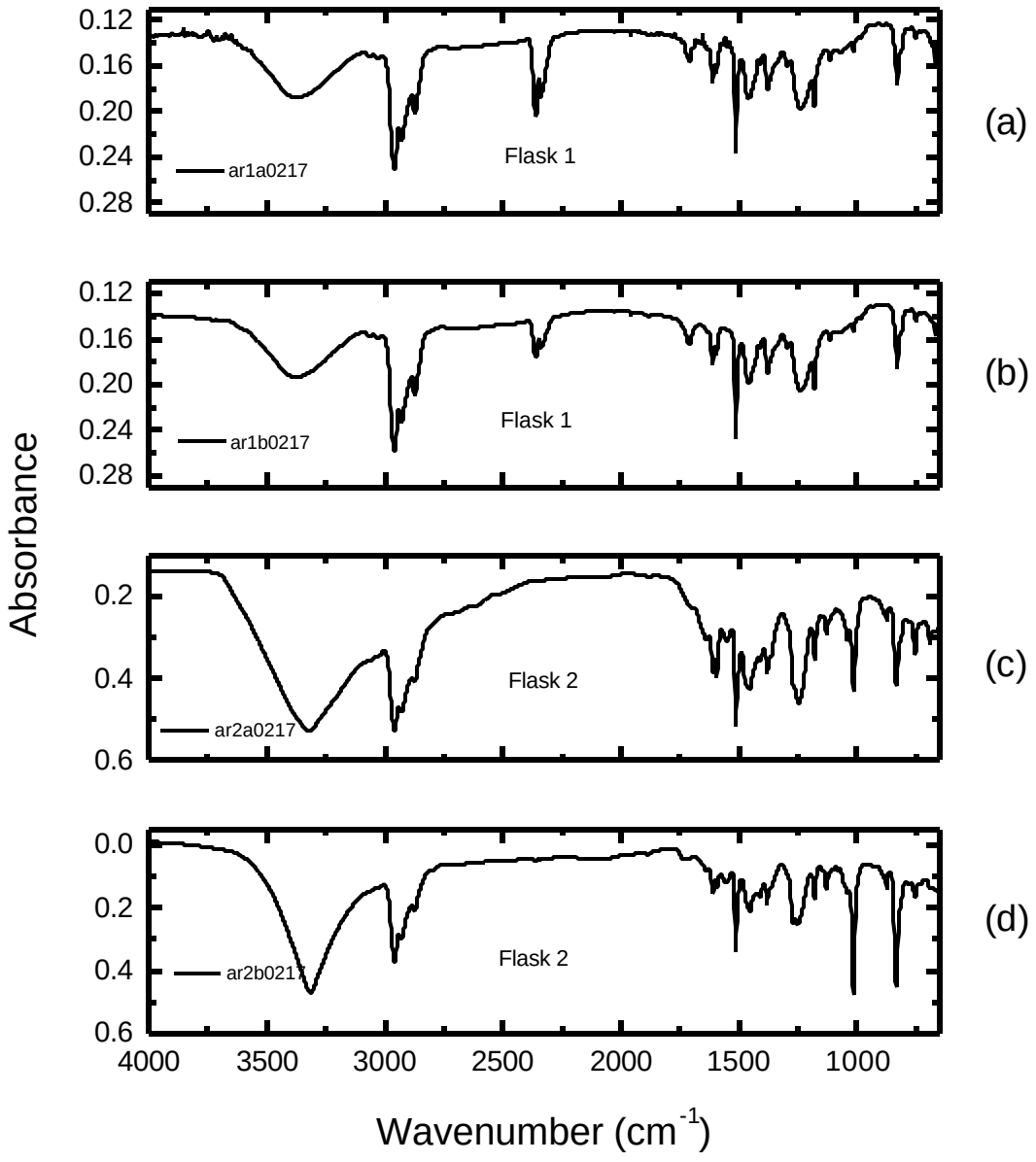

Fig. 40. FTIR spectra from condensable fractions collected during Experiment 021799 with EF-AR20 foam: (a) Flask 1, (b) Flask 1, (c) Flask 2, and (d) Flask 2.

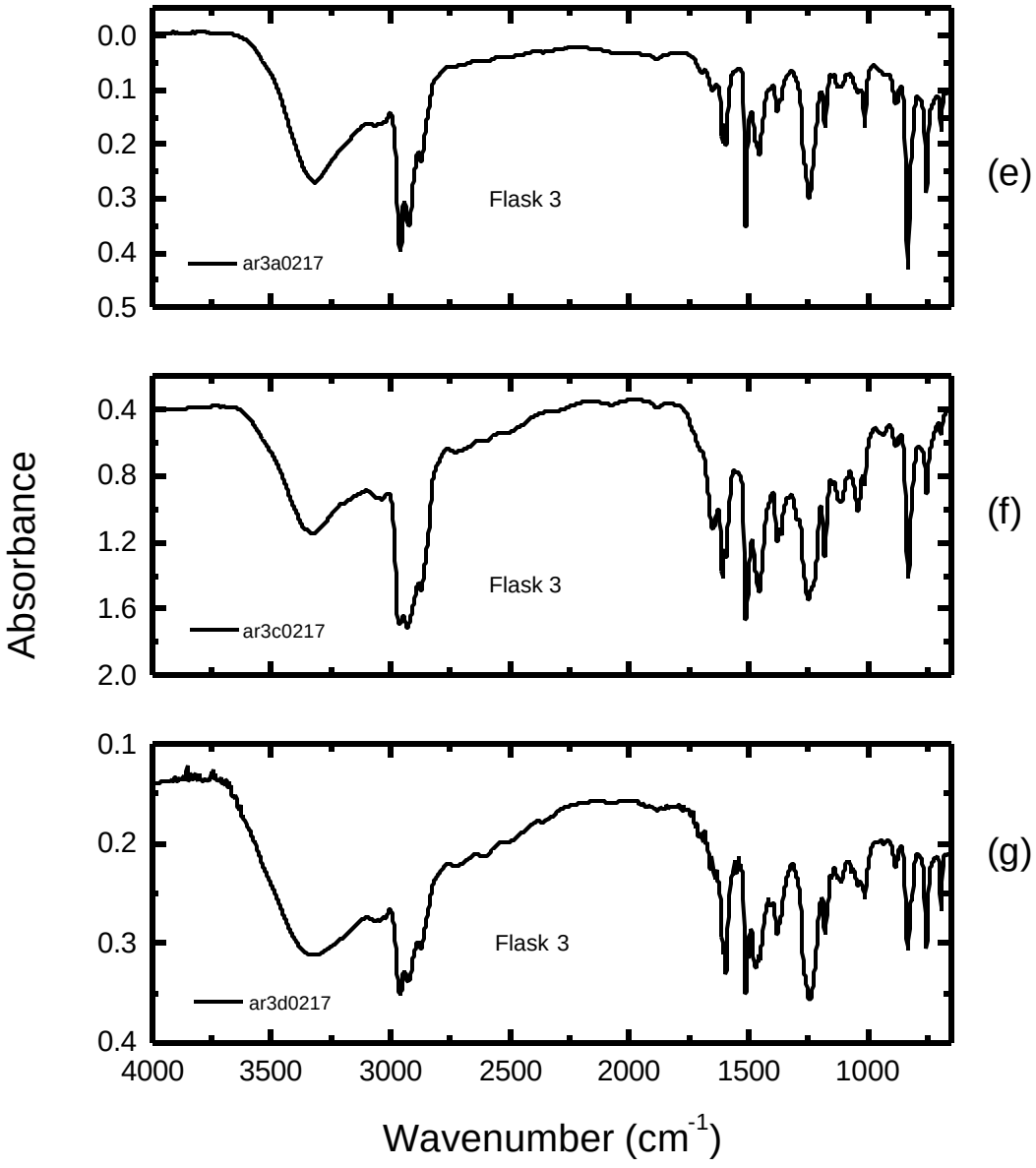

Fig. 40 cont'd. FTIR spectra from condensable fractions collected during Experiment 02179 with EF-AR20 foam: (e) Flask 3, (f) Flask 3, and (g) Flask 3.

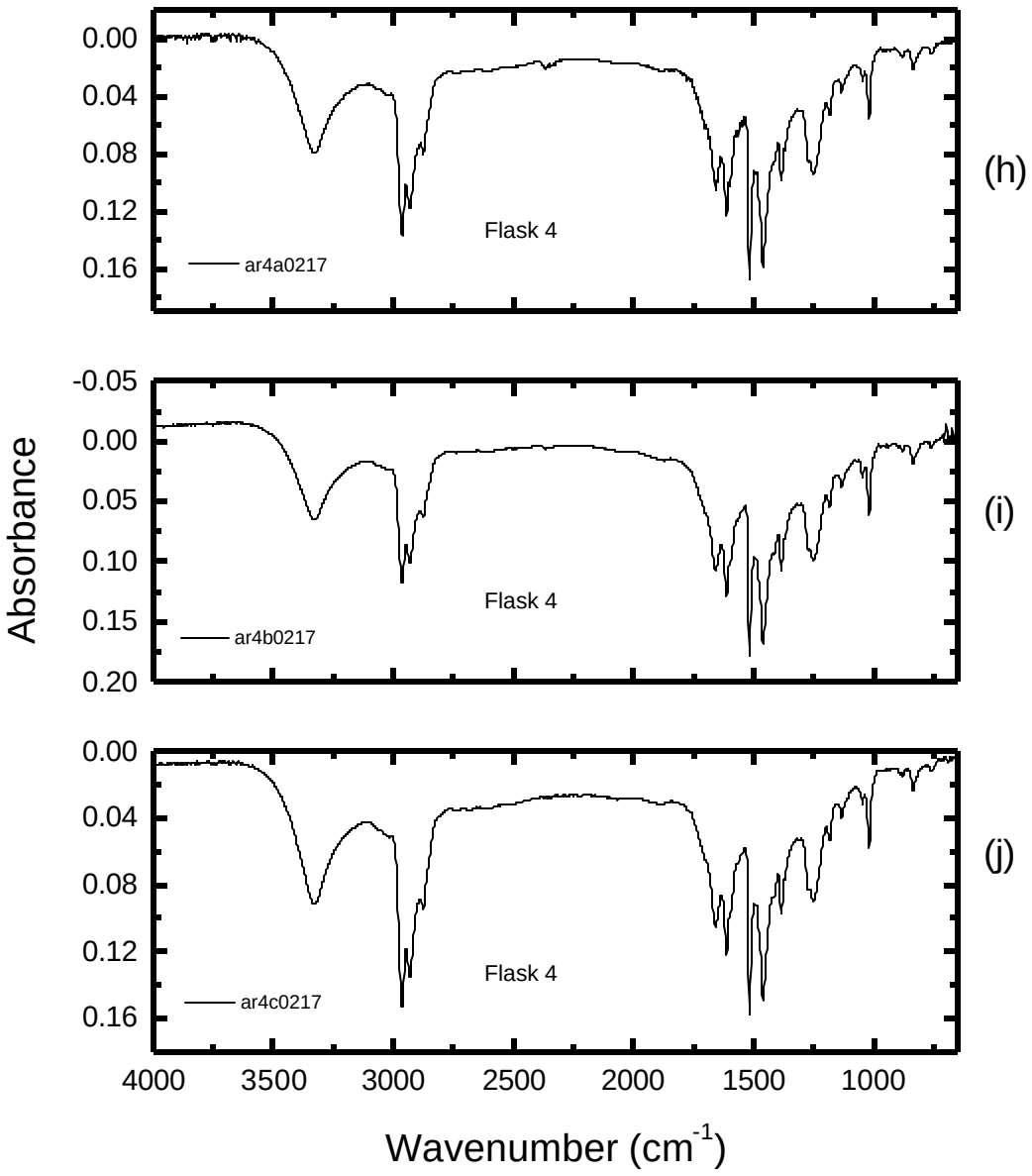

Fig. 40 cont'd. FtIR spectra from condensable fractions collected during Experiment 021799 with EF-AR20 foam: (h) Flask 4), (i) Flask 4, and (j) Flask 4.

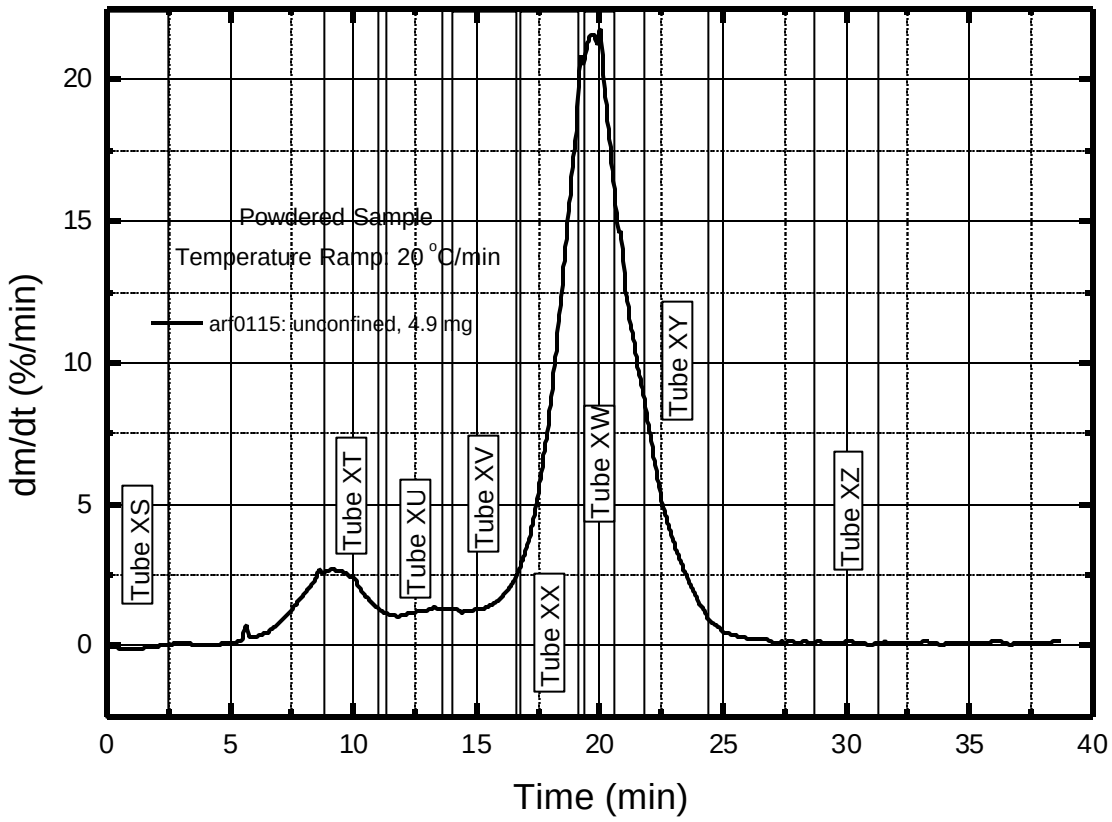

Fig. 41. Desorption tube sample points for GC-MS analysis of EF-AR20 based on TGA data profile.

DISTRIBUTION

Brigham Young University
Department of Chemical Engineering
Attn: Daniel Clayton (1)
Dr. Thomas H. Fletcher (1)
350 K Clyde Building
Provo, Utah 84602-4100

Sandia

1	MS0821	L. A. Gritzo, 9132
1	MS0824	J. L. Moya, 9130
1	MS0824	A. C. Ratzel, 9110
1	MS0826	W. Hermina, 9113
1	MS0828	K. J. Dowding, 9133
1	MS0828	J. T. Nakos, 9132
1	MS0828	M. Pilch, 9133
1	MS0834	T. Y. Chu, 9100
1	MS0834	J. N. Castaneda, 9112
15	MS0834	K. L. Erickson, 9112
1	MS0834	M. R. Prairie, 9112
1	MS0834	J. E. Johannes, 9114
1	MS0834	A. C. Sun, 9114
1	MS0835	S. N. Kempka, 9141
1	MS0835	J. M. McGlaun, 9140
1	MS0836	B. L. Bainbridge, 9116
1	MS0836	B. D. Boughton, 9116
1	MS0836	D. D. Dobranich, 9116
1	MS0836	E. Hertel, 9116
1	MS0836	M. L. Hobbs, 9116
1	MS0836	R. E. Hogan, 9116
1	MS0836	L. G. Minier, 9116
1	MS0836	C. Romero, 9116
1	MS0836	R. G. Schmidt, 9116
1	MS0836	W. Gill, 9132
1	MS0841	T. C. Bickel, 9100
3	MS0886	T. T. Borek, 1822
1	MS0886	R. P. Goehner, 1822
1	MS0888	R. L. Clough, 1811
1	MS0888	E. M. Russick, 1811
3	MS1202	T. A. Ulibarri, 5932
1	MS1411	D. K. Derzon, 1811
1	MS1454	J. C. Miller, 2554
3	MS1454	A. M. Renlund, 2554

1	MS9018	Central Technical Files, 8945-1
2	MS0899	Technical Library, 9616
1	MS0612	Review and Approval Desk, 9612 for DOE/OSTI